Journal of Materials Chemistry C

Accepted Manuscript

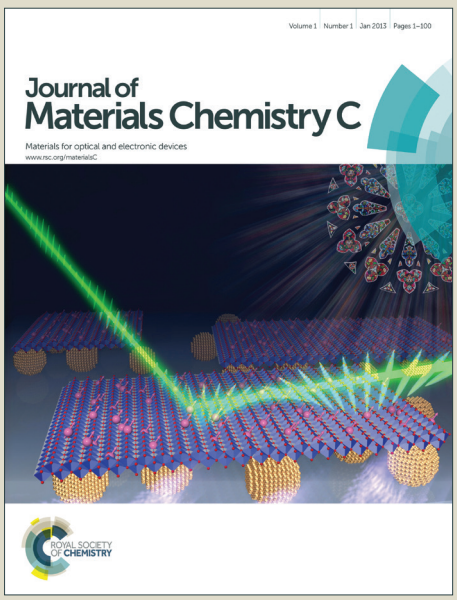

ROYAL SOCIETY OF CHEMISTRY

www.rsc.org/materialsC

Phosphine Oxide Functionalized Pyrenes as Efficient Blue Light Emitting Multifunctional Materials For Organic Light Emitting Diodes

Godumala Mallesham,[1,2] Chidirala Swetha,[1,2] Surukonti Niveditha,[2] Maneesha Esther Mohanty,[1] Nanubolu Jagadeesh Babu,[3,*] Arunandan Kumar,[4,*] Kotamarthi Bhanuprakash [2,5,*] and Vaidya Jayathirtha Rao ,[1,5,*]

[1]Crop Protection Chemicals Division, CSIR-Indian Institute of Chemical Technology, Hyderabad 500007, India, E-mail: jrao@iict.res.in

[2]Inorganic and Physical Chemistry Division, CSIR-Indian Institute of Chemical Technology, Hyderabad 500007, India, E-mail: bhanu2505@yahoo.co.in

[3]Centre for X-ray Crystallography, CSIR-Indian Institute of Chemical Technology, Hyderabad 500007, India, E-mail: jagadeesh.nanubolu@iict.res.in

[4]Laboratoire Interdisciplinaire Carnot de Bourgogne (ICB) UMR 6303 CNRS, Universit´e de Bourgogne. 9, Av. Savary, BP 47870, 21078 Dijon Cedex, France.
E-mail: kumar.arunandan@gmail.com

[5]Network Institute for Solar Energy, New Delhi, India

ABSTRACT

Aiming for blue light emitting multifunctional materials, electron transport enhancing diphenylphosphine-oxide (Ph_2P=O) group is appended to blue light emitting pyrene derivatives. This design, we observe, leads to highly efficient electron transporting blue-emitters for non-doped organic light emitting devices (OLEDs) with good film formation characteristics the superior performance attributed to enhanced charge transport and formation of pyrene excimers assisted by thermally activated delayed fluorescence (TADF) in the device. We report the synthesis and characterization using experimental and computational methods of six such pyrene derivatives. Although three of these derivatives show quenching of luminescence in solvents at higher concentrations, in the thin film invariably all six of them exhibit typical pyrene excimer emission. X-ray crystal analysis reveal π–π stacking and the C-H···O interactions in the solid due to P=O group. The measured electron mobilities for all the compounds are higher in comparison to standard electron transport material Alq_3. Non-doped OLEDs with the pyrene derivatives as emitters (multi layer configuration) as well as an electron transport cum emitters (bilayer configuration) exhibit excellent efficiencies. The derivatives as electron transporting emitters exhibit a performance with current efficiency (η_c) in the range 21.1–30.1 cd/A, power efficiency (η_p) 11.0–15.76 lm/W, external quantum efficiency (EQE) 3.0–4.0% and brightness 28500–42750 cd/m^2. In addition, the derivatives as emitter demonstrate very good external quantum efficiency in the range of 7.2–9.1%. These results demonstrate a successful strategy to obtain blue light emitting multifunctional materials for OLED applications.

KEYWORDS: *synthesis of pyrene-phosphine oxides, thermally activated delayed fluorescence (TADF), pyrene excimers, electron transport and emitting materials, organic light emitting devices.*

INTRODUCTION

Organic molecules with potential applications as luminescent materials have been the focus of current research because of the attractive custom tailored design and versatility of synthesis. An example of a practical application of such a molecule as a material is the emissive layer in organic light emitting diodes (OLED). Since the initial report, there has been a rapid progress of research in the field of OLED both at the basic and applied level.[1] OLEDs have potential as a technology for flat panel displays and lighting because of their characteristic low driving voltage, high brightness, full-colour emission, fast response time, wide viewing angle and self-emitting properties with an added advantage of low price.[2] Full colour displays require the three primary colours (red, green and blue) with equal stability, colour purity and improved efficiency.[3] Among these, green and red light emitters have been extensively studied and numerous reports are available in the literature.[4] However, blue light emitting materials are relatively less explored due to their wide band gap and low HOMO energy level which impede the charge carrier injection from the adjacent layers.[5] Thus, the development of blue light emitting materials with high efficiency remains as a challenge to researchers.

The basic OLED principle is that the hole (radical cation) and electron (radical anion) should undergo recombination in emissive layer (electrochemiluminescence (ECL)) to generate light.[6] Generally, OLEDs with fluorescent and phosphorescent

emitters have been fabricated in multilayer configuration, possessing hole transport layer (HTL), an emitting layer (EML) and an electron transport layer (ETL) along with charge injection and blocking layers which are sequentially deposited in between anode and cathode with each layer having their own functioning.[6] In such configuration, holes and electrons are injected from HTL and ETL, respectively into the emitting layer, where the charge recombination takes place and an exciton is generated which emits light. The major drawbacks of the multilayer configuration are the complexity and manufacturing cost.[7] To overcome these hurdles, materials with multi functional properties, like emission and charge transport have to be developed so as to reduce the number of layers in the device.[8] Emitting materials with electron transport property are relatively less explored than hole transporting emitters.[9] Though the phosphorescent OLEDs show high efficiency compared to fluorescent OLEDs, the colour purity, dopant concentration and triplet-triplet annihilations limit their applications.[10] Recently Adachi and co-workers[11-16] have identified a new phenomenon that thermally activated delayed fluorescence(TADF) can play a major role in enhancing the performance of OLEDs. Overall small organic molecules have advantages like easy synthesis and purification over polymers.

Keeping the above factors in mind and our own research interest, we aim in this work to develop an efficient multifunctional blue emitter.[9c,17] We chose pyrene moiety for the emitting part because of its high fluorescence quantum yield, good thermal stability and more active positions to develop numerous analogues.[18] Though pyrene as an emitter has been a subject of numerous investigations, most of the reported work has focused on preventing its tendency to form $\pi-\pi$ stacking and excimers.[19] Very few

reports actually utilize the excimer emission of pyrene in the device.[20] As the π–π stacking enhances the charge transport we retain it and additionally we increase the electron affinity of the molecules by end capping electron deficient/withdrawing diphenyl phosphine oxide group to the pyrenes. In an earlier study, end capping pyrene derivatives with electron donating diarylamino groups to obtain bifunctional blue emitting material yielded reduced EL.[19l] On the other hand there are reports of P=O functional group appended to highly fluorescent molecules like anthracene and triphenylamine leading to effective electron transporting blue emitters. [21]

Using this design principle, here we have synthesized and investigated six new diphenyl phosphine-oxide appended pyrene derivatives (Figure 1). In this series of compounds, different spacers were introduced to compound **10** to improve optical and thermal properties. The positional isomers **11** and **13** were designed to verify the influence of molecular configuration on optoelectronic properties. The increase in number of phenyl rings between pyrene and PO entities offers to increase the thermal stability. Compound **15** was designed to compare the influence of non planar biphenyl and planar flourene motif as π–bridge. Two methyl groups were appended on phenyl ring which cause molecular non planarity through twisting of phenyl ring for compound **14**. Photophysical, electrochemical and thermal properties evaluation of all the compounds (**10**-**15**) have been carried out. The crystal structure of **13** was analyzed by X-ray crystallography. Non-doped OLEDs were fabricated for the compounds **10-15** as an emitter [device configuration: ITO (120 nm)/F_4-TCNQ (2.5 nm)/*α*-NPD (45 nm)/emissive layer (**10-15**) (30 nm)/BCP (6 nm)/Alq_3 (30 nm)/LiF (1 nm)/Al (150 nm)] as well as an electron transport emitter [device configuration: ITO (120 nm)/F_4-TCNQ (2.5

nm)/*α*-NPD (45 nm)/emissive layer (**10-15**) (50 nm)/LiF (1 nm)/Al (150 nm)]. In addition, the electron mobilities were measured for all the compounds at an electric field of $1x10^5$ V/cm. To the best of our knowledge the present manuscript is the first report of phosphine oxide functionalized pyrene derivatives as multifunctional blue light emitters.

Results and Discussion

Synthesis and Characterization

Scheme 1 and Scheme 2 illustrate the synthetic sequence adopted to obtain the target materials **10-15** (Figure 1). Pyrene was brominated to get bromo pyrene **1**[30] and subsequently **1** was transformed to its corresponding borolane derivative **2**[31] (Scheme 1). In another sequence commercially available fluorene was brominated to get dibromo derivative **3**[32] and further it was dimethylated to obtain compound **4**[33] (Scheme 1). Suzuki-Miyaura coupling reaction was developed to make key mono bromo intermediates **5-9** in good yields (73-85%), by reacting compound **2** with various dibromo derivatives like 1,4-dibromobenzene, 4,4'-dibromobiphenyl, 1,3-dibromobenzene, 1,4-dibromo-2,5-dimethylbenzene and 2,7-dibromo-9,9-dimethyl-9H-fluorene (Scheme 2).[34] The synthesized mono bromo intermediates **1** and **5-9** were treated with *n*-BuLi to generate corresponding aryl lithio derivative at -78 ^oC, quenched with chlorodiphenylphosphine and subsequently oxidized using hydrogen peroxide to obtain target phosphine oxide compounds (**10-15**) as depicted in Scheme 2. All the intermediates and target compounds were characterized by ^1H, ^{13}C NMR, and mass spectrometry techniques. The target compounds (**10-15**) were additionally characterized by ^{31}P NMR, EI-HRMS and IR-spectroscopic studies (see experimental section).

Molecular Geometry, Orbital Picture and Crystal Structure

Knowledge of the geometry of the individual molecules would be of help in understanding the properties and also the effect of substitution. Additionally comparison of the geometries obtained by X-ray analysis where possible (molecule in solid state environment), and DFT methods (isolated molecules in gas phase) would also be helpful in understanding the intermolecular interactions in the solid. In this study only for **13** we were able to determine the molecular structure using X-ray analysis shown in Figure 2 along with the DFT optimized structure. From the Figure 2 it can be seen that the major changes in the geometry on changing the environment from solid to gas phase are the dihedral angles between the rings (Table S1-Supporting Information). The dihedral angle between the pyrene ring and the neighbouring aryl ring is about 10° smaller in the gas phase but larger changes of as much as 70° are seen in the dihedral angles of the phenyl groups in the diphenylphosphine oxide moiety. This indicates the large role of the P=O moiety in the stabilization of molecules in solid state. [22]

Another important point is to understand the conjugation between the pyrene ring and the phosphine oxide group in the ground state. In case of **13** in spite of the smaller dihedral angle of 55° between the pyrene ring and the phenyl group one can observe that due to *m*-substitution of the diphenyl phosphine oxide group the conjugation is decreased. But for all the other molecules the dihedral angle between the pyrene ring and its neighbouring group dictates the conjugation. For example in **14** the optimized angle is 75° which is large and attributed to the steric effect, we can expect a decreased conjugation. On the other hand in **11, 12** and **15** the angles vary between smaller values namely, 35°-55° indicating conjugation would be effective. Thus for all the molecules this

dihedral angle seems to play an important role in enhancing or decreasing the charge transfer.

The frontier molecular orbitals along with the individual contributions of the groups are shown in Figure 3. In all the molecules, the HOMO is mostly localized on the pyrene ring. While the LUMO of **10**, **13** and **14** are mainly localized on the pyrene ring, in the case of **11**, **12** and **15** the LUMO is delocalized on the non pyrene part due to conjugation. The dipole moments estimated from DFT studies indicate that the ground state dipole moments are small ~ 3.4–4.0 Debye (Table 1) with very little variation with substitution.

We also obtain other near degenerate conformations with different dihedral angles between the pyrene ring and the neighbouring aryl ring when we change our initial geometry in the DFT methods shown as isomer 2 for **13** (Figure S1- Supporting Information). In fact one can envisage many near degenerate local minima (rotational conformations) due to the low rotation barrier about of this angle in these molecules in the gas and solvent phase in the ground states. In the excited state too one can expect say in the case of intramolecular charge transfer a change in the geometry due to this dihedral angle. But this rotation may be restricted in the solid state due to the strong intermolecular forces.

To get a deeper understanding of the intermolecular interactions we study the solid state nature of **13** (Figure 4). **13** crystallizes in the triclinic $P\bar{1}$ space group with a single molecule in the asymmetric unit (Z' = 1). The molecule is predominantly hydrophobic due to the polar phosphine oxide. This functional group is considered to be

a good H-bond acceptor and can result in strong hydrogen bonding usually with polar amine or hydroxyl donor groups. However in **13**, the phosphine oxide involves in multiple C-H···O interactions because the molecule lacks strong hydrogen bond donors. Three C-H···O interactions essentially propagate the molecular packing and stabilize the crystal lattice - a C2-H2···O1 interaction with its inversion related molecule facilitates dimer formation, followed by extending the dimer of molecules into a ziz-zag tape via C30-H30···O1 interaction, and finally by linking inversion related tapes by a third C15-H15···O1 interaction. The pyrene rings allow multiple π–π ring stacking interactions to be established along the zig-zag tape and render additional stability to the crystal structure. Significant non-covalent interactions in **13** along with their symmetry codes are tabulated (Table S2- Supporting Information).

Electrochemical Properties

The redox behaviour of **10-15** was investigated by performing cyclic voltammetric (CV) experiments with a standard three-electrode configuration electrochemical cell in dry THF under nitrogen atmosphere, and ferrocene as the internal reference (Figure S2- Supporting Information). The main aim is to estimate the ionization potential (IP) and the electron affinity (EA) values of the molecules relative to the vacuum level. The IP of all the compounds are estimated (after correcting for the ferrocene standard) from the onset oxidation potential according to an empirical formula IP = $-(E_{ox}^{onset} + 4.8)$ eV[35] and EA are estimated from the onset reduction potentials according to an empirical formula EA = $-(E_{red}^{onset} + 4.8)$ eV[35] which are compiled in Table 1. Their potentials were corrected to the saturated calomel electrode (SCE) by measuring the

ferrocene/ferrocenium couple in this system (0.6 V versus SCE). The onset oxidation potentials of **10-15** are estimated to be between 1.26–1.46 V corresponding to the IP between 5.46–5.66 eV. The very little variation indicates that the oxidation occurs from the same moiety in all the molecules, namely pyrene. The onset reduction potentials are estimated to be between 1.6–1.85 V which corresponding to the EA of 2.35-2.60 eV. For comparison, the EA of Alq_3, an electron transport material, is 3.0 eV. [9b] The band gaps obtained by the electrochemical methods are in the range 2.95-3.24 eV (Table 1).

IP and EA estimated by CV can be correlated to the HOMO and LUMO energy values obtained from DFT calculations.[36] Hence, to compare the DFT obtained frontier orbital data is given in the same Table. While the HOMO values obtained from DFT are in good agreement with the IP obtained from CV measurements, the LUMO values are slightly underestimated by the DFT method. While it is well known that EA using DFT methods are underestimated, additionally here this could be also due to different conformation adapted by the molecule in the solvent (variation of LUMO is larger with change in geometry in these molecules).[37] Figure 5 depicts the typical energy level diagram for a bilayer device with α-NPD as HTL and synthesized materials as n-type emitter. IP of compounds offers a minimal energy barrier for holes to be injected from α-NPD, while EA is relatively closer to the work function of cathode LiF/Al. Hence, the compounds are suitable for hole and electron injection.

Photophysical Properties

UV-Vis absorption studies have been carried out for **10-15** in chloroform (1.0 x 10^{-5} M) as well as in thin film state to analyze the optical properties and to estimate their utility for EL applications. The corresponding spectra are shown in Figure 6 and the relevant data is summarized in Table 2. The absorption spectra of **10**-**15** are almost similar having comparable high energy bands (~260–300 nm) and low energy bands (~325–350 nm). There is very little variation of the λ_{max} with substitution (346-353 nm) indicating that the group causing this absorption in all the molecules is most probably same. **10** and **14** exhibit fine structure (relative to **11**, **12**, **13** and **15**) in their absorption spectra. To understand the nature of the band solvatochromic studies in various non-polar to polar solvents were carried out. Small or negligible solvent polarity effect was observed in the UV-Vis absorption spectra of these compounds (Table S3 and Figure S3-Supporting Information), indicating that there is no major change in the dipole moment of these molecules upon excitation. In the case of the thin films, the absorption spectra recorded are almost similar to the absorption spectra in solution as shown in the same figure, except for a small red shift. This red shift (~10 nm) can be attributed to the intermolecular interactions like π–π stacking or due to change in the dihedral angle in the solid state.

TD-DFT calculations at pbe0/6-31g (d,p)[22] level of theory have been carried out to get deeper insight into the absorption spectra and to know the origin of electronic transitions. The absorption maxima obtained by computational methods are in good agreement with the experimental values (Table 2). First singlet excited state (S_1) of all the molecules is attributed to the HOMO-LUMO transition (~90%). From the orbitals

shown in Figure 3 this could be classified as $\pi - \pi^*$ transition. Interestingly in the case of **10, 13** and **14** the orbital density is almost localized on the pyrene moiety in the HOMO-LUMO transition, while in the rest of the molecules the HOMO-LUMO transition proceeds with a small charge transfer to the neighbouring aryl moiety. This can be seen in the computed oscillator strengths of the transitions which are slightly smaller in the case **10, 13** and **14**.

Fluorescence spectra of **10**-**15** were recorded in chloroform solvent as well as in the thin film. The spectra are shown in Figure 6 and the relevant data summarized in Table 2. The emissions in chloroform are in the range of 380-420 nm which can be attributed to substituted pyrene monomer. The fluorescence quantum yield (Φ_f) of the derivatives **10-15** were measured in $CHCl_3$ using quinine sulphate (quantum yield: 0.53)[23] as standard (Table 2) and are in the range of 0.51-0.91. Optical band gaps obtained from the intersection point of offset point of absorption and onset of emission are given in the same Table. The band gaps lie in the region 3.10-3.38 eV corresponding to blue emission. Interestingly the spectra of **11, 12** and **15** in chloroform show a broad structureless peak having a small red shift compared to **10, 13** and **14**. The emission in the thin film state of all the molecules are red shifted to around 458-482 nm. This large red shift can occur due to aggregation in the solid state or due to change in geometry of the molecules in the solid state.

Fluorescence spectra were also recorded in various polar and non polar solvents to understand the nature of the excited state (Table 3 and Figure S4-Supporting Information). Fluorescence spectra recorded for **11**, **12** and **15** in various solvents show a red shift of almost 20-30 nm in going from hexane to a more polar solvent

acetonitrile/methanol. This behaviour is absent in **10**, **13** and **14** which exhibit almost no red shift. The possible reason for this is that the former molecules are excited to a local excited state (HOMO-LUMO) which then relaxes to an intramolecular charge transfer state (ICT) with change in the geometry. On the other hand in **10, 13** and **14** the excited state do not show any charge transfer with the charge being localized almost on the pyrene moiety even after excitation.

Changes in the emission spectra with increasing concentration of the compound were also studied in chloroform solvent (Figure S5-Supporting Information). With increasing concentration the intensity of the emission spectra of **13** at 390 nm decreases, and a new peak at 430 nm is observed which increases in intensity with increasing concentration. This effect is also seen in **10** and **14** where the red shifted peaks are at 430 and 420 nm, respectively. The emission spectra of **10**, **13** and **14** at low energy wavelength in thin film are similar in high concentration solution spectra and different in low concentration solution, which can be attributed to emission from pyrene excimer. In fact the thin film emission has a broad emission, typical of excimer emission.

On the other hand in **11, 12** and **15** with increasing concentration in the solvent, self quenching is observed. The intensity of the peak decreases with no formation of a new red shifted peak. In the corresponding thin film spectra, we find that there are broad peaks around 450-470 nm like in the case of **10, 13** and **14**. Based on the red shift and the previous data of **10, 13** and **14** we believe this emission to be also due to the formation of excimers. The quenching effect in the solvent could be caused by change in geometry (ICT) in the excimer on excitation (rotation of the pyrene ring) leading to non radiative decay of the excited state. On the other hand, the strong intermolecular

interactions restrict the rotation in the solid which leads to a radiative decay. Thus, we attribute that the emissions 450-482 nm in the solid in all the molecules **10-15** arising due to the excimer emission. Importantly, all the compounds exhibit their emission in the blue region (380-480 nm) in solution as well as in thin film state.

To understand the mechanism of luminiscence and also to identify the species responsible for emission, luminiscence lifetime measurements were carried out for compound **13**. Femto laser set up was used to determine the short lived fluorescence lifetimes for **13**. In lower concentration (10^{-5} M) where the steady state data shows no excimer formation, the short lifetime component (5ns) may be attributed to the lifetime of the locally excited singlet state and the longer lifetime (12 ns) to charge separation between pyrene and diphenyl phospheneoxide. Fluorolog3 spectrometer equipped with flash lamp was used for determining delayed emission for **13**. The fluorescence lifetime decay of **13** at 10^{-5} and 10^{-2} M concentrations was measured at emission wavelength 390 and 460 nm (Table-S4, Figure S6-supporting information). Delayed emission of **13** was checked with 0.1 ms delay after flash, the spectra shows delayed emission with a lifetime of 9 μs at lower concentration (10^{-5} M), at higher concentration (10^{-2} M) 7 μs and 97 μs (Figure 7) involving excimer formation. The delayed emission with 9 μs life time is the delayed fluorescence of **13**, since it has overlap with the fluorescence spectrum of **13**. The origin of this delayed fluorescence is interesting that it arises from a possible close lying triplet.[11-16] Both fluorescence and delayed fluorescence spectra are nearly coincident hence the delayed component maybe attributed to thermally activated delayed fluorescence.[38,39] The proposal of close lying triplet comes from the observations recorded on phosphine oxide containing small molecules[40] having triplet

energy, E_T ~3.1 eV. The singlet formed upon absorption of light undergoes inter system crossing to give triplet state, which undergoes reverse intersystem crossing (RISC) to populate delayed singlet leading to delayed fluorescence (Figure 7) or it can interact with another molecule (at higher concentrations) leading to excimer fluorescence. The reverse intersystem crossing associated with TADF arises due to close lying singlet and triplet states.

Thermal Properties

Thermogravimetric analysis (TGA) and differential scanning calorimetry (DSC) measurements were carried for **10-15** to obtain thermal decomposition (T_d) and glass transition temperatures (T_g), respectively (Figure S7 –Supporting Information). The obtained T_d and T_g data are presented in Table 4. The compounds **10-15** exhibit good thermal stability with T_d (corresponding to 5% weight loss) in the range of 341-444 ^oC. In a repeated DSC scans, relatively high T_g values were observed in second heating scan and are in between 73 –125 ^oC. Among the six compounds, high T_g values were noticed for **12** (104 ^oC), **14** (112 ^oC) and **15** (125 ^oC) than other compounds (**10**, **11** and **13**), which could be attributed to the increased molecular size and molecular weight. Crystallization temperature as exothermic peak in DSC scans was not observed for all the compounds indicating their amorphous nature, which is required for better performance of OLEDs. Melting points exhibited in DSC scans as sharp endothermic peaks were found to be in between 188 – 273 ^oC.

Electroluminescent (EL) Properties

EL studies were performed for **10**-**15** using them as electron transport emitters with the following configuration (i): ITO (120 nm) F_4-TCNQ (2.5 nm)/*α*-NPD (45 nm)/emissive layer **10**-**15** (50 nm)/LiF (1 nm)/Al (150 nm). In this device, ITO (indium tin oxide) and LiF/Al are the anode and the cathode, respectively; *α*-NPD (4,4'-bis[N-(1-naphthyl)-N-phenyl amino] biphenyl) is the hole transporting layer (HTL). The F_4-TCNQ (2,3,5,6-tetrafluoro-7,7',8,8'-tetracyanoquinodimethane) is utilized for efficient hole injection from ITO to *α*-NPD and its thickness is used as optimized by Priyanka Tyagi[41] *et al* for enhanced efficiency and life time of OLEDs. Then the EL spectrum, Current density – Voltage – Luminescence (J-V-L) characteristics and CIE co-ordinates are characterized by EL devices. Figure 8 depicts the EL spectrum for all the molecules and their emission was found to be in 465-491 nm wavelength range. Peak wavelength and CIE co-ordinates for each device are listed in Table 5. J-V-L characteristics of the bilayer devices using these molecules as emitter are presented in Figure 9. The EL devices constructed using **10**-**15** as emitters show good EL performance over a wide range of current density. The current and power efficiency were calculated for each device and are tabulated in Table 5. The onset voltage and maximum brightness data have also been included in the same Table. All the devices were found to possess very low onset voltage, 3.5 V. The key point to be noted about the device is that these devices are not having any doped transport layer. Therefore, the onset voltage of 3.5 V indicates very high electron mobilities for these molecules. This also indicates charge carrier balance inside the emissive layer. Bilayer devices are found to possess very high brightness around 30,000 cd/m^2. The efficiency of these devices are found to be very high with current efficiency (η_c) ~16.0 cd/A and power efficiency (η_c) ~8.0 lm/W. The high

efficiency data indicate that these molecules have very high electron mobilities and emission efficiencies. Further, we have also measured the external quantum efficiencies for these devices at 6.0 V. The quantum efficiencies are found to be in the range of 3.0–4.0% and these quantum efficiencies are very high for bilayer blue fluorescent OLEDs. If a 1:3 ratio of singlet to triplet excitons [4c,d] and 20% out coupling efficiency for OLED structure is considered [41b,c], the internal quantum efficiency of these OLEDs comes in the range of 60–80%, which is very close to the measured fluorescence efficiencies for these molecules. Therefore, these bilayer devices have charge carrier balance factor very close to unity, which indicates the electron mobility of these molecules is very close to the hole mobility in *α*-NPD.[41d]

Furthermore, to have a complete analysis of the EL properties of these molecules, we also tested them as an emitter with a multilayer device structure as (ii): ITO (120 nm)/F_4-TCNQ (2.5 nm)/*α*-NPD (45 nm)/Emissive layer **10**-**15** (30 nm)/BCP (6 nm)/Alq_3 (30 nm)/LiF (1 nm)/Al (150 nm), which has an additional BCP as hole blocking layer and Alq_3 electron transport layer.[41e-g] Figure 10 depicts the J-L characteristics for these devices. The efficiency data are listed in the Table 6. Multilayer OLEDs show very high efficiencies as close to 16 lm/W power efficiency, 45 Cd/A current efficiency and 9.1% external quantum efficiency. From this data, it can be seen that the results of these compounds as electron transporting emitters are very close to results as emitters. The difference in the efficiency data is nearly two times for multilayer device in comparison to bilayer as compared to the previous reports on emitting organic molecules it is nearly 5-10 times.[9b,42] For reference, the OLED with Alq_3 as emissive layer with the same structure has power efficiency close to 2 lm/W and pyrene

derivative in same configuration, the efficiency goes as high as to 10 lm/W and gives a difference in efficiency by a factor of 5.[43] This indicates that our molecules possess very high electron mobility in comparison to Alq_3. Therefore, in configuration (i), the injected electrons into the emitting molecules from cathode traversed very quickly to the HTL/EML interface, where the recombination zone is located and high fluorescence efficiencies of these molecules give rise to very high luminous efficiencies of the devices. Hence, these molecules serve the purpose of both electron transport as well as emission. The selected thickness was 50 nm which leads to a recombination zone located near the HTL/EML interface to avoid cathode induced quenching, as obtained by other researchers.[44] Recently reported efficiencies (external quantum) for synthesized blue emitters are 2.4% based on carbozole-dimesitylborane by Lin et al,[45a] 5.0% on triphenylamine-imidazole by Li et al,[45b] 3.1% and 2.0 % by Zhang et al[45c] and Yu et al[45d]. The other reports also range from 3.0-6.0%[45e,f]. The higher reported efficiencies in our case clearly signify the improvement made in our synthesized compounds.

We have measured the electron mobilities of these molecules using time of flight method.[46] The electron mobilities are found to be in the range of $1x10^{-4} – 5x10^{-4}$ cm^2/Vs measured at an electric field of $1x10^5$ V/cm (Table 5). To understand the reason for the high values, we carry out the calculation of the transfer integrals, using computational chemistry, between the molecules in the crystal of **13** and for comparison in an unsubstituted pyrene crystal obtained from literature (Figure 11).[47] The values of the transfer integral for both electron and hole transport in the unsubstituted pyrene is large but only in one direction, while from the figure it is clear that the charge transport in **13**

has more possible channels with slightly smaller transfer integrals. This increase in channels we believe leads to larger electron mobilities. These results justify our arguments for the high efficiencies as electron transport emitters. The measured mobilities in our molecules were found to be an order of magnitude higher than the standard electron transport material Alq_3.[41h, 46] Also from the electron mobility data, the low efficiencies in case of **14** can be explained. This molecule was found to have a three times lower mobility in comparison to other materials and therefore, give rise to low efficiencies due to a charge carrier balance factor less than unity. These EL studies infer that the molecules synthesized in these studies possess excellent n-type emitting properties.

EXPERIMENTAL SECTION

Synthesis and Characterization:

Various mono bromo intermediates (**5**-**9**) were synthesized using Suzuki-Miyaura coupling reaction and were further used to attain target phosphine oxide derivatives (**10**-**15**).

Synthesis of 1-(4-bromophenyl)pyrene (5)

1,4-Dibromobenzene (3.0 g, 12.8 mmol), compound **2** (3.8 g, 11.5 mmol), and $Pd(PPh_3)_4$ catalyst (0.74 g, 0.6 mmol) were mixed in toluene (80 mL). Aqueous K_2CO_3 (5.2 g, 38.5 mmol) was slowly added to the reaction mixture and nitrogen gas was purged for 30 min. The reaction mixture was heated to reflux for 12 h under nitrogen

atmosphere (reaction progress was monitored by TLC). After completion of the reaction, it was diluted with ethyl acetate (150 mL). Organic layer was washed with brine solution, water, dried over anhydrous Na_2SO_4, filtered and the solvent was removed *in vacuo*. The residue was purified by column chromatography using *n*-hexane as eluent to afford compound **5** as colourless solid. Yield: 83% (3.4 g); mp 142-144 ^oC; ^1H NMR (300 MHz, $CDCl_3$, δ): 8.18 (d, *J* = 7.9 Hz, 2H), 8.16-8.09 (m, 2H), 8.07 (s, 2H), 8.03-7.96 (m, 2H), 7.90 (d, *J* = 7.9 Hz, 1H), 7.67 (d, *J* = 8.3 Hz, 2H), 7.47 (d, *J* = 8.3 Hz, 2H); ^{13}C NMR (75 MHz, $CDCl_3$, δ): 144.87, 136.05, 133.09, 132.13, 131.99, 131.92, 131.26, 130.88, 130.71, 130.53, 128.58, 128.44, 128.21, 127.80, 127.68, 127.25, 127.18, 126.04, 125.26, 124.97, 124.77, 124.57; EI-MS: *m/z* 356 $[M]^+$.

Synthesis of 1-(4'-bromobiphenyl-4-yl)pyrene (6)

Compound **6** was synthesized according the procedure similar to that of compound **5**, using 4,4'-dibromobiphenyl (3.0 g, 9.7 mmol) and compound **2** (2.8 g, 8.7 mmol) as synthetic precursors, $Pd(PPh_3)_4$ (0.56 g, 0.5 mmol) as catalyst and K_2CO_3 (3.9 g, 29.0 mmol) as base. The obtained residue was purified by column chromatography using chloroform: hexane (1:20) as eluent. Yield 80% (3.0 g); mp 217-220 ^oC; ^1H NMR (300 MHz, $CDCl_3$, δ): 8.28-8.16 (m, 4H), 8.13-8.10 (m, 2H), 8.08-8.00 (m, 3H), 7.79-7.69 (m, 4H), 7.66-7.57 (m, 4H); EI-MS: *m/z* 434 $[M]^+$.

Synthesis of 1-(3-bromophenyl)pyrene (7)

Compound **7** was synthesized according the procedure similar to that of compound **5**, using 1,3-dibromobenzene (3.0 g, 12.8 mmol) and compound **2** (3.8 g, 11.5 mmol) as synthetic precursors, $Pd(PPh_3)_4$ (0.74 g, 0.6 mmol) as catalyst and K_2CO_3 (5.2 g, 38.5

mmol) as base. The obtained residue was purified by column chromatography using hexane as eluent. Yield 85% (3.5 g); mp 125-127 ^{o}C; ^{1}H NMR (300 MHz, $CDCl_3$, δ): 8.21 (d, *J* = 7.8 Hz, 2H), 8.17 (d, *J* = 7.8 Hz, 1H), 8.13-8.07 (m, 3H), 8.06-8.00 (m, 2H), 7.93 (d, *J* = 7.9 Hz, 1H), 7.79 (t, *J* = 1.5 Hz, 1H), 7.60 (d, *J* = 8.1 Hz, 1H), 7.55 (d, *J* = 7.6 Hz, 1H), 7.42 (t, *J* = 7.8 Hz, 1H); ^{13}C NMR (75 MHz, $CDCl_3$, δ): 143.26, 135.85, 133.33, 131.35, 130.85, 130.81, 130.23, 129.80, 129.21, 128.33, 127.80, 127.64, 127.38, 127.27, 126.05, 125.28, 124.99, 124.82, 124.72, 124.67, 124.57, 122.44; EI-MS: *m/z* 356 $[M]^+$.

Synthesis of 1-(4-bromo-2,5-dimethylphenyl)pyrene (8)

Compound **8** was synthesized according the procedure similar to that of compound **5**, using 1,4-dibromo-2,5-dimethylbenzene (3.0 g, 11.4 mmol) and compound **2** (3.4 g, 10.3 mmol) as synthetic precursors, $Pd(PPh_3)_4$ (0.66 g, 0.6 mmol) as catalyst and K_2CO_3 (5.2 g, 38.5 mmol) as base. The obtained residue was purified by column chromatography using hexane as eluent. Yield 73% (2.9 g); mp 119-121 ^{o}C; ^{1}H NMR (300 MHz, $CDCl_3$, δ): 8.17 (d, *J* = 7.9 Hz, 2H), 8.16-8.11 (m, 1H), 8.07 (s, 2H), 8.01-7.93 (m, 2H), 7.80 (d, *J* = 7.7 Hz, 1H), 7.68 (d, *J* = 9.1 Hz, 1H), 7.56 (s, 1H), 7.21 (s, 1H), 2.43 (s, 3H), 1.96 (s, 3H); ^{13}C NMR (75 MHz, $CDCl_3$, δ): 139.86, 136.36, 136.04, 134.88, 133.38, 132.87, 131.33, 130.89, 130.62, 128.77, 127.60, 127.38, 127.35, 127.09, 126.02, 125.17, 125.08, 124.99, 124.73, 124.66, 124.50, 123.91, 22.38, 19.47; EI-MS: *m/z* 384 $[M]^+$.

Synthesis of 1-(7-bromo-9,9-dimethyl-9H-fluoren-2-yl)pyrene (9)

Compound **9** was synthesized according the procedure similar to that of compound **5**, using compound **4** (3.0 g, 8.6 mmol) and compound **2** (2.5 g, 7.7 mmol) as synthetic precursors, $Pd(PPh_3)_4$ (0.49 g, 0.4 mmol) as catalyst and K_2CO_3 (3.5 g, 25.7 mmol) as base. The obtained residue was purified by column chromatography using hexane as eluent. Yield 85% (3.1 g); mp 186-188 ^oC; ^1H NMR (300 MHz, $CDCl_3$, δ): 8.25 (d, *J* = 2.0 Hz, 1H), 8.24 (d, *J* = 3.4 Hz, 1H), 8.21 (dd, *J* = 7.6, 1.1 Hz, 1H), 8.17 (d, *J* = 7.6 Hz, 1H), 8.11 (d, *J* = 0.6 Hz, 2H), 8.06-8.01 (m, 3H), 7.86 (d, *J* = 7.8 Hz, 1H), 7.70-7.66 (m, 2H), 7.64-7.61 (m, 2H), 7.52 (dd, *J* = 8.1, 1.8 Hz, 1H), 1.57 (s, 6H); ^{13}C NMR (75 MHz, $CDCl_3$, δ): 155.89, 153.43, 140.63, 137.90, 137.82, 137.20, 131.43, 130.89, 130.54, 130.19, 129.74, 128.46, 127.60, 127.51, 127.38, 126.19, 125.99, 125.16, 125.12, 124.88, 124.79, 124.63, 121.47, 121.13, 119.88, 47.23, 27.04; EI-MS: *m/z* 474 $[M]^+$.

Synthesis of diphenyl(pyren-1-yl)phosphine oxide (10)

To a suspension of **1** (3.0 g, 10.7 mmol) in dry THF (120 mL) was added *n*-BuLi (6.4 mL, 12.8 mmol, 2.0 M in cyclo hexane) drop wise at -78 ^oC, under nitrogen atmosphere, which turns to a greenish suspension. Stirring was continued for another 1 h, and then chlorodiphenylphosphine (3.0 mL, 16.1 mmol) was added drop wise while maintaining the same temperature, the reaction mixture turned to clear pale yellow solution. The resulting mixture was gradually warmed to ambient temperature, stirred for 2 h. After completion of the reaction (monitored by TLC), dry methanol (10 mL) was added. The organic compound was extracted with dichloromethane (3 x 80 mL), and the combined organic layer was dried over sodium sulphate, filtered and evaporated under reduced pressure to get white solid. The residue obtained was dissolved in dichloromethane (50 mL) and H_2O_2 (10 mL, 30%) was added dropwise. After stirring for 4 h at room

temperature, water (60 mL) was added and the organic phase was extracted with dichloromethane (3 x 40 mL), dried over anhydrous Na_2SO_4, filtered and the solvent was removed *in vacuo*. The crude reaction mixture was purified by column chromatography using hexane: ethyl acetate (1:1) as eluent to afford compound **10** which further purified by precipitating in chloroform and diethyl ether (1:3) mixture. Yield 68% (3.2 g); mp 243 ^{o}C; ^{1}H NMR (300 MHz, $CDCl_3$, δ): 8.93 (d, *J* = 9.1 Hz, 1H), 8.27-8.15 (m, 3H), 8.11-8.00 (m, 4H), 7.80-7.67 (m, 5H), 7.60-7.52 (m, 2H), 7.51-7.42 (m, 4H); ^{13}C NMR (75 MHz, $CDCl_3$, δ): 134.16, 133.89, 132.50, 132.22, 132.09, 131.85, 131.22, 131.06, 130.94, 130.34, 129.82, 128.87, 128.66, 128.50, 127.06, 126.44, 126.28, 126.15, 123.59, 123.41; ^{31}P NMR (500 MHz, $CDCl_3$, δ): 32.886; IR (KBr, cm^{-1}): 3049, 1585, 1187, 847, 695; EI-MS: *m/z* 402 $[M]^+$; EI-HRMS: *m/z* Calcd for $C_{28}H_{19}OP$: 402.11735 $[M]^+$; found: 402.11720; UV-Vis ($CHCl_3$, nm) (ε, M^{-1} cm^{-1}): 271 (36177), 282 (57035), 325 (18305), 339 (37890), 353 (52457), 379 (8534).

Synthesis of diphenyl(4-(pyren-1-yl)phenyl)phosphine oxide (11)

Compound **11** was prepared according the procedure similar to that of **10**, using **5** (2.5 g, 7.0 mmol), *n*-BuLi (4.2 mL, 8.4 mmol, 2.0 M in cyclohexane) and chlorodiphenylphosphine (1.9 mL, 10.5 mmol) as synthetic precursors. The obtained residue was purified by column chromatography (hexane/ethyl acetate 1:1) followed by precipitation in chloroform: diethyl ether (1:3). Yield 72% (2.4 g); mp 208 ^{o}C; ^{1}H NMR (300 MHz, $CDCl_3$, δ): 8.19 (t, *J* = 7.8 Hz, 2H), 8.15 (d, *J* = 7.5 Hz, 1H), 8.11 (d, *J* = 9.2 Hz, 1H), 8.07 (d, *J* = 1.4 Hz, 2H), 8.03-7.98 (m, 2H), 7.93 (d, *J* = 7.8 Hz, 1H), 7.88-7.78 (m, 6H), 7.72 (dd, *J* = 8.1, 2.4 Hz, 2H), 7.60-7.50 (m, 6H); ^{13}C NMR (75 MHz, $CDCl_3$, δ):

144.98, 144.95, 136.13, 133.20, 132.17, 132.04, 131.98, 131.82, 131.34, 130.94, 130.78, 130.73, 130.57, 128.62, 128.46, 128.28, 127.83, 127.72, 127.28, 127.24, 126.07, 125.32, 125.00, 124.85, 124.70, 124.62; ^{31}P NMR (500 MHz, $CDCl_3$, δ): 29.141; IR (KBr, cm^{-1}): 3041, 1589, 1197, 831, 692; EI-MS: *m/z* 478 $[M]^+$; EI-HRMS: *m/z* Calcd for $C_{34}H_{23}OP$: 478.14865 $[M]^+$; found: 478.14809; UV-Vis ($CHCl_3$, nm) (ε, M^{-1} cm^{-1}): 270 (33937), 281 (49877), 330 (28075), 346 (44332).

Synthesis of diphenyl(4'-(pyren-1-yl)-[1,1'-biphenyl]-4-yl)phosphine oxide (12)

Compound **12** was prepared according the procedure similar to that of **10**, using **6** (2.5 g, 5.8 mmol), *n*-BuLi (3.5 mL, 6.9 mmol, 2.0 M in cyclohexane) and chlorodiphenylphosphine (1.6 mL, 8.7 mmol) as synthetic precursors. The obtained residue was purified by column chromatography (hexane/ethyl acetate 1:1) followed by precipitation in chloroform: diethyl ether (1:3). Yield 75% (2.4 g); mp 244 ^{o}C; ^{1}H NMR (300 MHz, $CDCl_3$, δ): 8.24-8.15 (m, 4H), 8.09 (s, 2H), 8.05-7.98 (m, 3H), 7.81-7.70 (m, 12H), 7.60-7.47 (m, 6H); ^{13}C NMR (75 MHz, $CDCl_3$, δ): 144.24, 141.11, 138.64, 136.85, 133.21, 132.74, 132.60, 132.15, 132.01, 131.41, 131.15, 130.88, 130.69, 130.50, 128.61, 128.45, 127.59, 127.51, 127.47, 127.34, 127.19, 127.03, 126.03, 125.18, 125.03, 124.87, 124.66; ^{31}P NMR (500 MHz, $CDCl_3$, δ): 28.996; IR (KBr, cm^{-1}): 3047, 1594, 1180, 849, 696; EI-MS: *m/z* 554 $[M]^+$; EI-HRMS: *m/z* Calcd for $C_{40}H_{27}OP$: 554.17995 $[M]^+$; found: 554.17986; UV-Vis ($CHCl_3$, nm) (ε, M^{-1} cm^{-1}): 269 (45661), 281 (66729), 330 (32635), 347 (53724).

Synthesis of diphenyl(3-(pyren-1-yl)phenyl)phosphine oxide (13)

Compound **13** was prepared according the procedure similar to that of **10,** using **7** (2.5 g, 7.0 mmol), *n*-BuLi (4.2 mL, 8.4 mmol, 2.0 M in cyclohexane) and chlorodiphenylphosphine (1.9 mL, 10.5 mmol) as synthetic precursors. The obtained residue was purified by column chromatography (hexane/ethylacetate 1:1) followed by precipitation in chloroform: diethyl ether (1:3). Yield 66% (2.2 g); mp 196 ^{o}C; ^{1}H NMR (300 MHz, $CDCl_3$, δ): 8.17 (d, *J* = 7.8 Hz, 2H), 8.14 (d, *J* = 7.8 Hz, 1H), 8.05 (d, *J* = 2.9 Hz, 2H), 8.03-7.93 (m, 3H), 7.91 (d, *J* = 7.8 Hz, 2H), 7.86-7.75 (m, 6H), 7.66 (td, *J* = 7.6, 2.9 Hz, 1H), 7.56-7.45 (m, 6H); ^{13}C NMR (75 MHz, $CDCl_3$, δ): 141.45, 141.36, 136.08, 134.07, 134.05, 133.92, 133.84, 133.37, 132.80, 132.55, 132.09, 132.01, 131.97, 131.95, 131.31, 130.93, 130.85, 130.80, 130.73, 128.61, 128.56, 128.52, 128.46, 128.25, 127.73, 127.62, 127.47, 127.23, 126.02, 125.25, 124.91, 124.79, 124.67, 124.59, 124.51; ^{31}P NMR (500 MHz, $CDCl_3$, δ): 29.01; IR (KBr, cm^{-1}): 3039, 1582, 1187, 851, 697; EI-MS: *m/z* 478 $[M]^+$; EI-HRMS; *m/z* Calcd for $C_{34}H_{23}OP$: 478.14865 $[M]^+$; found: 478.14852; UV-Vis ($CHCl_3$, nm) (ε, M^{-1} cm^{-1}): 272 (38723), 281 (57657), 330 (33286), 348 (45803).

Synthesis of (2,5-dimethyl-4-(pyren-1-yl)phenyl)diphenylphosphine oxide (14)

Compound **14** was prepared according the procedure similar to that of **10**, using **8** (2.5 g, 6.5 mmol), *n*-BuLi (3.9 mL, 7.8 mmol, 2.0 M in cyclohexane) and chlorodiphenylphosphine (1.8 mL, 9.8 mmol) as synthetic precursors. The obtained residue was purified by column chromatography (hexane/ethyl acetate 1:1) and was further purified by precipitating in chloroform: diethyl ether (1:3). Yield 58% (1.9 g); mp 188 ^{o}C; ^{1}H NMR (300 MHz, $CDCl_3$, δ): 8.21 (t, *J* = 7.9 Hz, 2H), 8.17 (d, *J* = 7.2 Hz, 1H),

8.10 (s, 2H), 8.03-7.99 (m, 2H), 7.84 (d, *J* = 7.9 Hz, 1H), 7.83-7.77 (m, 4H), 7.67 (d, *J* = 9.1 Hz, 1H), 7.61-7.50 (m, 6H), 7.31 (d, *J* = 4.3 Hz, 1H), 7.09 (d, *J* = 14.3 Hz, 1H), 2.47 (s, 3H), 1.90 (s, 3H); ^{13}C NMR (75 MHz, $CDCl_3$, δ): 144.58, 140.10, 139.99, 135.91, 135.07, 134.92, 134.28, 134.14, 133.96, 133.79, 133.56, 132.19, 132.04, 131.93, 131.78, 131.26, 130.82, 130.68, 128.64, 128.47, 127.68, 127.45, 127.27, 126.69, 126.02, 125.21, 125.03, 124.92, 124.45, 21.23, 19.75; IR (KBr, cm^{-1}): 3048, 2917,1598, 1186, 848, 717; EI-MS: *m/z* 506 [M^+]; EI-HRMS: *m/z* Calcd for $C_{36}H_{27}OP$: 506.17995 $[M]^+$; found: 506.17775; UV-Vis ($CHCl_3$, nm) (ε, M^{-1} cm^{-1}): 269 (42209), 279 (67110), 315 (18706), 330 (41780), 345 (59413).

Synthesis of (9,9-dimethyl-7-(pyren-1-yl)-9H-fluoren-2-yl)diphenylphosphine oxide (15)

Compound **15** was prepared according the procedure similar to that of **10**, using **9** (2.5 g, 5.3 mmol), *n*-BuLi (3.2 mL, 6.3 mmol, 2.0 M in cyclohexane) and chlorodiphenylphosphine (1.5 mL, 7.9 mmol) as synthetic precursors. The obtained residue was purified by column chromatography (hexane/ethyl acetate 1:1) followed by precipitation in chloroform: diethyl ether (1:3). Yield 79% (2.5 g); mp 273 ^{o}C; ^{1}H NMR (300 MHz, $CDCl_3$, δ): 8.22 (d, *J* = 9.1 Hz, 2H), 8.18 (d, *J* = 7.6 Hz, 1H), 8.15 (d, *J* = 7.6 Hz, 1H), 8.08 (s, 2H), 8.05-7.97 (m, 4H), 7.90 (d, *J* = 7.6 Hz, 1H), 7.82 (dd, *J* = 7.8, 2.3 Hz, 1H), 7.78-7.70 (m, 5H), 7.62 (d, *J* = 7.8 Hz, 1H), 7.58-7.46 (m, 7H), 1.56 (s, 6H); ^{13}C NMR (75 MHz, $CDCl_3$, δ): 154.52, 154.10, 153.94, 142.69, 141.48, 137.59, 136.87, 133.51, 132.10, 131.97, 131.84, 131.35, 131.27, 131.19, 130.81, 130.54, 129.88, 129.74, 128.50, 128.35, 127.52, 127.39, 127.30, 126.46, 126.34, 125.95, 125.09,

125.01, 124.97, 124.77, 124.58, 120.54, 119.86, 119.68, 47.28, 26.90; ^{31}P NMR (500 MHz, $CDCl_3$, δ): 29.932; IR (KBr, cm^{-1}): 3038, 2961, 1598, 1434, 1192, 844, 696; EI-MS: *m/z* 594 $[M]^+$; EI-HRMS: *m/z* Calcd for $C_{43}H_{31}OP$: 594.21125 $[M]^+$; found: 594.21218; UV-Vis ($CHCl_3$, nm) (ε, M^{-1} cm^{-1}): 268 (27423), 280 (38296), 312 (29979), 351 (45056).

Measurements

All chemicals are reagent/analytical grade and used without further purification. ^{1}H NMR and ^{13}C NMR were recorded on a Bruker Avance (75 MHz) spectrometer in $CDCl_3$ with TMS as the internal standard. ^{31}P NMR spectra were recorded on Avance *III*-500 MHz spectrometer in $CDCl_3$ with reference to phosphoric acid. Mass spectra obtained by using electron ionization (EI) ion trap mass spectrometry (Thermofinnigan, Sanzox, CA, USA) were recorded on a VG-AUTOSPEC spectrometer. Elemental analyses were performed using a Vario-EL elemental analyzer. UV-Vis absorption spectra were measured using a Jasco V-550 spectrophotometer. Steady state fluorescence spectra were recorded using a Spex Fluorolog-3 spectrofluorometer. The fluorescence quantum yields (Φ_f) were estimated by integrating the fluorescence bands and by using quinine sulphate as the standard.[17] The glass-transition temperature (T_g) of the compounds were measured using differential scanning calorimetry (DSC) under a nitrogen atmosphere and at a heating rate of 10 °C min^{-1} using a DSC Q200 (TA instruments). The T_g was determined from the second heating scan. Thermogravimetric analysis (TGA) was performed using a TGA/SDTA 851e (Mettler Toledo) in the temperature range of 30–550 °C under a nitrogen atmosphere at a heating rate of 10 °C min^{-1}. Cyclic voltammetric measurements were performed on a PC-controlled CHI 620C electrochemical analyzer (CH instruments). Cyclic voltammetric experiments were

performed in 1 mM solution of degassed dry THF at a scan rate of 100 mV s^{-1} using 0.1 M tetrabutylammoniumperchlorate (TBAP) as the supporting electrolyte. The glassy carbon was used as the working electrode, Ag/AgCl as the reference electrode and platinum wire as the counter electrode. The working electrode surface was first polished with 1 mm alumina slurry, followed by 0.3 mm alumina slurry on a micro cloth. It was then rinsed with Millipore water and also sonicated in water for 5 min. The polishing and sonication steps were repeated twice.

Fluorescence lifetime measurements

Steady state and time resolved phosphorescence measurements were carried out in Fluorolog-3 spectrofluorometer using flash lamp with 0.1 ms delay after flash at RT. Time correlated single photon counting was used to measure the fluorescence lifetime in the nanosecond time scale. The femtosecond pulses at 8 MHz repetition rate were obtained from fractional part of MaiTai output passing through femtosecond Pulse Selector (3980-5S, Spectra Physics). The excitation pulses at 370 nm were generated by frequency doubling the 740nm Ti-sapphire output with 0.5 mm BBO crystal. This excitation pulses are focused to the sample using Fluorescence Up-conversion set up (FOG100 system CDP System). The time distribution data of fluorescence intensity were recorded on a SPC-130 TCSPC module (Becker & Hickl).The instrument response function was 250 ps.

Crystal Structure Determination

The pyrene derivative **13** was crystallized from CH_3OH–$CHCl_3$ (1: 4) and the single crystal structure was determined. It crystallizes into the monoclinic P21/c space group. All H atoms were positioned geometrically and treated as riding on their parent C atoms, with C-H distances of 0.93-0.97 Å, and with $U_{iso}(H) = 1.2U_{eq}$ (C) or $1.5U_{eq}$ for methyl atoms. Crystal data for **13**: $C_{34}H_{23}OP$, M = 478.49, colourless needle, 0.42 x 0.12 x 0.10 mm^3, triclinic, space group P-1 (No. 2), a = 9.0088(9), b = 9.6445(9), c = 14.0042(13) Å, α = 96.309(2), β = 98.1750(10), γ = 92.359(2)°, V = 1195.1(2) $Å^3$, Z = 2, D_c = 1.330 g/cm^3, F_{000} = 500, CCD area detector, MoKα radiation, λ = 0.71073 Å, T = 293(2)K, $2\theta_{max}$ = 50.0°, 11563 reflections collected, 4195 unique (R_{int} = 0.0174). Final *GooF* = 1.062, *R1* = 0.0350, *wR2* = 0.1011, *R* indices based on 3860 reflections with I >2σ(I) (refinement on F^2), 325 parameters, μ = 0.142 mm^{-1}. CCDC 979234 contains the supplementary crystallographic data for this paper.[18]

Computational Methodology

To analyse the absorption spectra and molecular orbitals, quantum chemical calculations have been carried out. Optimized geometries of the molecules were obtained using density functional theory (DFT), at B3LYP/6-311g(d,p)[25] level of theory as implemented in the *Gaussian09*[26] software package. Frequency calculations were carried out to ensure that the minima obtained is a stationary point on the potential energy surface. Molecular orbital surfaces are visualized using *Gaussview*. Solvent effects are simulated using polarizable continuum model (PCM).[27] Lowest singlet excitation energies are calculated using time dependent density functional theory

(TDDFT) at pbe0/6-31g(d,p)[28] level of theory, in $CHCl_3$ solvent. The transfer integrals have been calculated at PW91/tzp level of theory using ADF software.[29]

Device Fabrication

For the EL studies, indium-tin oxide (ITO) coated glass substrates, with a sheet resistance of 20 Ω, were photo lithographically patterned and cleaned using trichloroethylene, acetone, and isopropyl alcohol and deionised water sequentially for 20 minutes using an ultrasonic bath and dried in flowing nitrogen. Prior to film deposition, the ITO substrates were treated with UV-ozone for 5 minutes. On the substrate, the hole transport layer, emitting layer, hole blocking layer, electron transport layer, electron injecting layer and cathode were sequentially deposited under a high vacuum (1×10^{-5} torr). The deposition rate of organic materials was kept at 1 Å s^{-1}, whereas the deposition rates of LiF and Al were 0.5 Å s^{-1} and 5 Å s^{-1} respectively. The thickness of the deposited layers was controlled by a quartz crystal monitor. The cathode was deposited on the top of the structure through a shadow mask. N,N-Diphenyl-N′,N′-bis(1-naphthyl)-1,1′-biphenyl-4,4′-diamine (*α*-NPD (Sigma Aldrich) was used as a hole transport layer, 2,9-dimethyl-4,7-diphenyl-1,10-phenanthroline (BCP) was used as hole blocking layer, tris(8-hydroxyquinoline)-aluminium (Alq_3, Sigma Aldrich) was used as an electron transport layer, LiF (Merck, Germany) was an electron injection layer and the Al as the cathode. The size of each pixel was 3–4 mm. The ECL spectra were measured using an Ocean Optics high resolution spectrometer (HR-2000CG UV-NIR). The J–V–L characteristics were measured with a luminance meter (LMT l-1009) and a Keithley 2400 programmable voltage–current digital source meter. All the measurements were carried out at room temperature under ambient conditions.

Conclusion

In summary, an effective strategy for the design of highly efficient multifunctional emitters with good film formation characteristics has been demonstrated. The high efficiencies of the compounds synthesized are explained on the basis of different phenomenon including charge transfer and delayed fluorescence. The $\pi-\pi$ stacking along with the other intermolecular interactions due to P=O group in the solid restrict the rotation of the pyrene molecules leading to blue emission of the pyrene excimer assisted by TADF in the excited state. These interactions also help in enhancing the electron and hole transport while the increased electron affinity due to diphenyl phosphine oxide group help in better electron injection. The present results demonstrate that these compounds are promising emitter cum electron-transport materials for OLEDs.

ACKNOWLEDGEMENTS

The authors, GM and SN thank UGC and MEM thanks CSIR-for SRA. We thank the Director, CSIR-IICT for the encouragement. We gratefully acknowledge CSIR for TAPSUN-NWP-0055 project funding.

References

1 C. W. Tang and S. A. Vanslyke, *Appl. Phys. Lett.,* 1987, **51**, 913.

2 J. H. Burroughs, D. D. C. Bradley, A. R. Broun, R. N. Marks, K. Mackay, R. H. Friend, P. L. Burn and A. B. Holmes, *Nature,* 1990, **347**, 539; b) J. Kido, M. Kumara and K. Nagai, *Science,* 1995, **267**, 1332; c) M. A. Baldo, M. E. Thompson and S. R. Forrest, *Nature,* 2000, **403**, 750; d) T. F. So, J. Kido and P. Burrows, *MRS Bull.,* 2008, **33**, 663; e) S. Reineke, F. Lindner, G. Schwartz, N. Seidler, K. Walzer, B. L. Ssem and K. Leo, *Nature,* 2009, **459**, 234; e) V. Jayathirtha Rao, G. Mallesham, G. S. Kumar and B. A. Rao, *Research signpost publications* 2013, ISBN 978-81-308-0508-5.

3 M. Zhu and C. Yang, *Chem. Soc. Rev.,* 2013, **42**, 4963.

4 a) C. Adachi, M.A. Baldo, S. R. Forrest, S. Lamansky, M. E. Thompson and R. C. Kwong, *Appl. Phys. Lett.,* 2001, **78**, 1622; (b) C. Adachi, R. C. Kwong, P. Djurovich, V. Adamovichi, M.A. Baldo, M.E. Thompson and S.R. Forrest, *Appl.Phys. Lett.,* 2001, **79**, 2082. (c) C. Adachi, M. A. Baldo, M. E. Thompson and S. R. Forrest, *J. Appl. Phys.,* 2001, **90**, 5048; d) Y. Sun, N. C. Giebink, H. Knanno, B. Ma, M. E. Thompson and S. R. Forrest, *Nature,* 2006, **440**, 908.

5 a) L. M. Leung, W. Y. Lo, S. K. So, K. M. Lee and W. K. Choi, *J. Am. Chem. Soc.,* 2000, **122**, 5640; b) L. H. Chan, R. H. Lee, C. F. Hsieh, H. C. Yeh and C. T. Chen, *J. Am, Chem. Soc.,* 2002, **124**, 6469; c) Y. H. Niu, B. Chen, T. D. Kim, M. S. Liu and A. K. Y. Jen, *Appl. Phys. Lett.,* 2004, **85**, 5433; d) M. T. Lee, C. H. Liao, C. H. Tasi and C. H. Chen, *Adv. Mater.,* 2005, **17**, 2493; e) R. C. Chiechi, R. J. Tseng, F.

Marchioni, Y. Yang and F. Wudl, *Adv. Mater*., 2006, **18**, 325; f) S. Tang, M. R. Liu, P. Lu, H. Xia, M. Li, Z. Q. Xie, F. Z. Shen, C. Gu, H. P. Wang, B. Yang and Y. Ma, *Adv. Funct. Mater.,* 2007, **17**, 2869; g) B. C. Krummacher, V. E. Choong, M. K. Mathsi, S. A. Choulis, F. Jermann, T. Fiedler and M. Zachau, *Appl. Phys. Lett*., 2006, **88**, 113506; h) Z. Q. Gao, Z. H. Li, P. F. Xia, M. S. Wong, K. W. Cheah and C. H. Chen, *Adv. Funct. Mater.,* 2007, **17**, 3194.

6 a) K.R.J. Thomas, J.T. Lin, Y.T. Tao and C.H. Chuen, *Chem. Mater*., 2004, 16, 5437; b) K.R.J. Thomas, M. Velusamy, J.T. Lin, C. H. Chuen and Y.T. Tao, *Chem. Mater.,* 2005, **17**, 1860; c) M. Gordon and W.R. Ware, *The Exciplex,* Academic Press, New York, 1975. d) Z. Li, H. Meng, LLC and Boca Raton, 2007. e) G. Zucchi, D. Tondelier, Y. Bonnassieux and B. Geffroy, *Polym. Int.,* 2014, **63***,* 1368.

7 Q. Tong, S. Lai, M. Chan, Y. Zhou, H. Kwong, C. Lee and S. Lee, *Chem. Mater.,* 2008, **20***,* 6310.

8 W. Hung, T. Tsai, S. Ku, L. Chi and K. Wong, *Phys. Chem. Chem. Phys.,* 2008, **10**, 5822.

9 a) C. Wang, G. Y. Jung, Y. Hua, C. Pearson, M. R. Bryce, M. C. Petty, A. S. Batsanov, A. E. Goeta and J. A. K. Howard, *Chem. Mater.,* 2001, **13**, 1167; b) A. P. Kulkarni, C. J. Tonzola, A. Babel and S. A. Jenekhe, *Chem. Mater.,* 2004, **16**, 4556; c) M. Ananth Reddy, A. Thomas, K. Srinivas, V. Jayathirtha Rao, K. Bhanuprakash, B. Sridhar, A. Kumar, M. N. Kamalasanan and R. Srivastava, *J. Mater. Chem.,* 2009, **19**, 6172.

10 a) M. A. Baldo, C. Adachi and S. R. Forrest, *Phys. Rev. B: Condens. Matter.,* 2000, **62**, 10967.

11 Q. Zhang, B. Li, S. Huang, H. Nomura1, H. Tanaka and Chihaya Adachi, *Nature photonics*, 2012, **8,** 326.

12 a) J. Lee, K. Shizu, H. Tanaka, H Nomura, T Yasuda and C. Adachi *J. Mater. Chem. C*, 2013, **1**, 4599; b) S Wu, M. Aonuma, Q. Zhang, S. Huang, T. Nakagawa, K. Kuwabara and C. Adachi, *J. Mater. Chem. C*, 2014, **2**, 421

13 Q. Zhang, J. Li, K. Shizu, S. Huang, S. Hirata, H. Miyazaki, and C. Adachi, J. Am. Chem. Soc. 2012, **134**, 14706.

14 S. Y. Lee, T. Yasuda, H. Nomura, and C. Adachi, *Appl. Phys. Lett*., 2012, **101**, 093306;

15 G. Mahes, H. Nomura, Q. Zhang, T. Nakagawa, and C. Adachi, Angew. Chem. Int. Ed. 2012, **51**, 11311;

16 T. Serevicius, T. Nakagawa, M.C. Kuo, S. H. Cheng, K. T. Wong, C. H. Chang, R. C. Kwong, S. Xia and Chihaya Adachi, *Phys. Chem. Chem. Phys.,* 2013, **15**, 15850;

17 a) G. Mallesham, S. Balaiah, M. Ananth Reddy, B. Sridhar, P. Singh, R. Srivastava, K. Bhanuprakash and V. Jayathirtha Rao, *Photochem. Photobiol. Sci.,* 2014, **13**, 342; b) M. Ananth Reddy, G. Mallesham, A Thomas, K. Srinivas, V. Jayathirtha Rao, K. Bhanuprakash, L. Giribabu, R. Grover, A. Kumar, M. N. Kamalasanan and R. Srivastava, *Synthetic Metals,* 2011, **161**, 869.

18 a) M. Teresa, F. Duarte. and K. Mullen. *Chem. Rev.,* 2011, **111**, 7260; b) G. Venugopal Rao, M. Janaki Ram Reddy, K. Srinivas, K. M. Bushan and V. Jayathirtha Rao, *Photochemistry and Photobiology,* 2002, **76**, 29; c) V. Raj Gopal, V. Jayathirtha Rao, G. Saroja and A. Samanta, *Chemical Physics Letters,* 1997,

270, 593; d) J. Y. Hu, Y. J. Pu, G. Nakata, S. Kawata, H. Sasabe and J. Kido, *Chem. Commun.,* 2012, **48**, 8434; e) X. Feng, F. Iwanaga, J. Y. Hu, H. Tomiyasu, M. Nakano, C. Redshaw, M. R. J. Elsegood and T. Yamato, *Org. Lett.,* 2013, **15**, 3594.

19 a) Z. Zhao, S. Chen, J. W. Y. Lam, P. Lu, Y. Zhong, K. S. Wong, H. S. Kwok and B. Z. Tang, *Chem. Commun.,* 2010, **46**, 2221; b) S. T. Tao, Z. K. Peng, X. H. Zhang, P. F. Wang, C.-S. Lee and S. T. Lee, *Adv. Funct. Mater.,* 2005, **15**, 1716; c) F. Liu, W. Y. Lai, C. Tang, H. B. Wu, Q. Q. Chen, B. Peng, W. Wei, W. Huang and Y. Cao, *Macromol. Rapid Commun*., 2008, **29**, 659; d) T. M. Figueira-Duarte, P. G. Del Rosso, R. Trattnig, S. Sax, E. J. W. List and K. Mullen, *Adv. Mater*., 2010, **22**, 990; e) C. Tang, F. Liu, Y. J. Xia, L. H. Xie, A. Wei, S.-B. Li, Q.-L. Fan and W. Huang, *J. Mater. Chem*., 2006, **16**, 4074; f) J. N. Moorthy, P. Natarajan, P. Venkatakrishnan, D.-F. Huang and T. J. Chow, *Org. Lett*., 2007, **9**, 5215; g) K. L. Chan, J. P. F. Lim, X. Yang, A. Dlapur, G. E. Jabbour and A. Sellinger, *Chem. Commun*., 2012, **48**, 5106; h) T. M. Figueira- Duarte, S. C. Simon, M. Wagner, S. I. Druzhinin, K. A. Zachariasse and K. Mullen, *Angew. Chem.,* 2008, **120**, 10329; i) Z. Zhao, J. H. Li, P. Lu and Y. Yang, *Adv. Funct. Mater*., 2007, **17**, 2203; j) J. Huang, X. Yang, J. Wang, C. Zhong, L. Wang, J. Qin and Z. Li, *J. Mater. Chem.,* 2012, **22**, 2478; k) J. Huang, N. Sun, J. Yang, R. Tang, Q. Li, D. Ma, J. Qin and Z. Li, *J. Mater. Chem*., 2012, **22**, 12001; l) W. L. Jia, T. McCormick, Q. D. Liu, H. Fukutani, M. Motala, R. Y. Wang, Y. Tao and S. Wang, *J. Mater. Chem.,* 2004, **14**, 3344.

20 a) K. C. Wu, P. J. Ku, C. S. Lin, H. T. Shih, F. I. Wu, M. J. Huang, J. J. Lin, I. C. Che and C. H. Cheng, *Adv. Funct. Mater*., 2008, **18**, 67; b) Z. F. Chang, S. H. Ye,

B. R. He, Z. R. Bei, L. Y. Lin, P. Lu, B. Chen, Z. J. Zhao and H. Y. Qiu, *Chem.–Asian J.*, 2013, **8**, 444.

21 a) C. H. Chien, C. K. Chen, F. M. Hsu, C. F. Shu, P. T. Chou and C. H. Lai, *Adv. Funct. Mater.,* 2009, **19**, 560; b) X. K. Liu, C. J. Zheng, M. F. Lo, J. Xiao, C. S. Lee, M. K. Fung and X. H. Zhang, *Chem. Commun.,* 2014, **50,** 2027.

22 a) A. B. Padmaperuma, L. S. Sapochak and P. E. Burrows, *Chem. Mater.*, 2006, **18**, 2389; b) P. Calcagno, B. M. Kariuki, S. J. Kitchin, J. M. A. Robinson, D. Philp and K. D. M. Harris, *Chem. Eur.J.*, 2000, **6**, 2338.

23 N. Demas and G. A. Crosby, *J. Phys. Chem.,* 1971,**76**, 1071.

24 These data can be obtained free of charge at www.ccdc.cam.ac.uk/conts/retrieving.html [or from the Cambridge Crystallographic Data Centre (CCDC), 12 Union Road, Cambridge CB2 1EZ, UK; fax: +44(0) 1223 336 033; email: deposit@ccdc.cam.ac.uk].

25 a) A. D. Becke, *J. Chem. Phys.,* 1993, **98**, 5648; b) A. D. Becke, *J. Chem. Phys.,* 1996, **104**, 1040; c) C. T. Lee, W. T. Yang and R. G. Parr, *Phys. Rev. B,* 1988, **37**,

26 *Gaussian 09*, Revision B.01, M. J. Frisch, G. W. Trucks, H. B. Schlegel, G. E. Scuseria, M. A. Robb, J. R. Cheeseman, G. Scalmani, V. Barone, B. Mennucci, G. A. Petersson, H. Nakatsuji, M. Caricato, X. Li, H. P. Hratchian, A. F. Izmaylov, J. Bloino, G. Zheng, J. L. Sonnenberg, M. Hada, M. Ehara, K. Toyota, R. Fukuda, J. Hasegawa, M. Ishida, T. Nakajima, Y. Honda, O. Kitao, H. Nakai, T. Vreven, Jr. J. A. Montgomery, J. E. Peralta, F. Ogliaro, M. Bearpark, J. J. Heyd, E. Brothers, K. N. Kudin, V. N. Staroverov, R. Kobayashi, J. Normand, K. Raghavachari, A. Rendell, J. C. Burant, S. S. Iyengar, J. Tomasi, M. Cossi, N. Rega, N. J. Millam, M.

Klene, J. E. Knox, J. B. Cross, V. Bakken, C. Adamo, J. Jaramillo, R. Gomperts, R. E. Stratmann, O. Yazyev, A. J. Austin,R. Cammi, C. Pomelli, J. W. Ochterski, R. L. Martin, K. Morokuma, V. G. Zakrzewski, G. A. Voth, P. Salvador, J. J. Dannenberg, S. Dapprich, A. D. Daniels, O. Farkas, J. B. Foresman, J. V. Ortiz,J. Cioslowski, D. J. Fox, Gaussian, Inc., Wallingford CT, 2010.

27 a) S. Miertuš, E. Scrocco and J. Tomasi, *Chem. Phys.,* 1981, **55**, 117; b) M. Cossi, V. Barone, R. Cammi and J. Tomasi, *Chem. Phys. Lett.,* 1996, **255**, 327.

28 a) J. P. Perdew, K. Burke and M. Ernzerhof, *Phys. Rev. Lett.*, 1996, **77**, 3865–3868; b) J. P. Perdew, K. Burke and M. Ernzerhof, *Phys. Rev. Lett.*, 1997, **78**, 1396–1396.

29 F. C. Grozema and *L. D. A.* Siebbeles, *Int. Rev. Phys. Chem.,* 2008, **27**, 87; b) E. F. Valeev, V. Coropceanu, D. A. da Silva, S. Salman and *J. L.* Bredas, *J. Am. Chem. Soc.,* 2006, **128**, 9882; c) G. Te Velde, F. M. Bickelhaupt, E. J. Baerends, C. Fonseca Guerra, S. J. A. Van Gisbergen, J. G. Snijders and T. Ziegler, *J. Comput. Chem***.,** 2001, **22**, 931.

30 a) P. V. Vyas, A. K. Bhatt, G. Ramachandraiah and A. V. Bedekar, *Tetrahedron Letters* 2003, **44**, 4085; b) M. Sharif, S. Reimann, K. Wittler, L. R. Knöpke, A. E. Surkus, C. Roth, A. Villinger, R. Ludwig and P. Langer, *Eur. J. Org. Chem.,* 2011, 5261.

31 a) C. He, Q. He, Q. Chen, L. Shi, H. Cao, J. Cheng, C. Deng and T. Lin, *Tetrahedron Lett.,* 2010, **51**, 1317; b) L. Yu, K. C. Lo, J. Xi, D. L. Phillips and W. K. Chan, *New J. Chem.,* 2013, **37**, 1833.

32 a) M. Ranger and M. Leclerc, *Can. J. Chem.,* 1998, **76**, 1571; b) D. W. Price, J. M.

Tour, *Tetrahedron,* 2003, **59***,* 3131.

33 G. Saroja, Z. Pingzhu, N. P. Ernsting, J. Liebscher, *J. Org. Chem.* 2004, **69**, 987.

34 a) A. Suzuki, *Pure Appl. Chem.* 1994, **66**, 213; b) J. Daub, R. Engl, J. Kurzawa, S. E. Miller, S. Schneider, A. Stockmann and M. R. Wasielewski, *J. Phys. Chem. A* 2001, **105**, 5655; c) C. Modrakowski, S. C. Flores, M. Beinhoff and A. D. Schlüter, *Synthesis*, 2001, **14,** 2143.

35 a) J. Pommerehne , H. Vestweber , W. Guss , R. F. Mahrt , H. Bässler , M. Porsch , J. Daub , *Adv. Mater.,* 1995, **7**, 551; b) A. J. Bard and L. R.Faulkner, *Electrochemical Methods - Fundamentals and Applications,* Wiley, New York, p. 634

36 J. L. Bredas, R. Silbey, D. S. Boudreaux and R. R. Chance, *J. Am. Chem. Soc.,* 1983, **105**, 6555.

37 G. Zhang and C. B. Musgrave . *J. Phys. Chem. A,* 2007, 111, **8**, 1554.

38 A. Endo, K. Sato, K. Yoshimura, T. Kai, A. Kawada, H. Miyazaki, and C. Adachi, *Appl. Phys. Lett.,* 2011, **98**, 083302.

39 T. Zhang, B. Chu, Wenlian Li, Z. Su, Q. M. Peng, o Zhao, Y. Luo,F. Jin, X. Yan, Y. Gao, Hairuo Wu, F. Zhang, D. Fan, and J. Wang, *ACS Appl. Mater. Interfaces,* 2014, **6**, 11907.

40 S. O. Jeon and J. Y. Lee, *J. Mater. Chem., 2012*, **22**, 4233.

41 a) P. Tyagi, A. Kumar, L. I. Giri, M. K. Dalai, S. Tuli, M. N. Kamalasanan and R. Srivastava, *Optics Letters*, 2013, **38**, 3854; b) K. Saxena, V. K. Jain and D. S. Mehta, *Opt. Mat., 2009*, **32**, 221; c) A. Kumar, R. Srivastava, P. Tyagi, D. S. Mehta and M. N. Kamalasanan, *Org. Elect., 2013*, **13**, 2879; d) K. Walzer, B. Maennig, M.

Pfeiffer and K. Leo, Chem. Rev., 2007, **107**, 1233; e) C.-T. Chen, *Chem. Mater.,* 2004, **16**, 4389; f) P. Tyagi, R. Srivastava , A. Kumar, G. Chauhan, A. Kumar, S. S. Bawa and M. N. Kamalasanan, *Syn. Met., 2010*, **160**, 1126; g) P. Tyagi, R. Srivastava, A. Kumar, V. K. Rai, R. Grover and M. N. Kamalasanan, Syn. Met., 2010, **160**, 756; h) P. Tyagi, R. Srivastava, A. Kumar, S. Tuli and M.N. Kamalasanan, *Org. Elect.*, 2013, **14**, 1391.

42 a) J.Y. Hu, Y.J. Pu, F. Satoh, S. Kawata, H. Katagiri, H. Sasabe and J. Kido, *Adv. Funct. Mater.,* 2014, **24**, 2064; b) Y.J. Pu, M. Yoshizaki, T. Akiniwa, K. Nakayama and J. Kido, *Organic Electronics,* 2009, **10**, 877; c) T. Oyamada, H. Sasabe and C. Adachi, *Applied Physics Letters,* 2005, **86**, 033503; d) J. Kido and Y. Okamoto, *Chem. Rev*., 2002, **102**, 2357; h) Y. Kijima, N. Asai and S.-i. Tamura, *Jpn. J. Appl. Phys.,* 1999, **38**, 5274.

43 J. Huang, M. Pfeiffer, A. Werner, J. Blochwitz, K. Leo and S. Liu, *Appl. Phys. Lett.,* 2002, **80**, 139.

44 a) A. L. Burin and M. A. Ratner, *J. Phys. Chem. A*, 2000, **104**, 4704; b) Y. Wu, Y. C. Zhou, H. R. Wu, Y. Q. Zhan, J. Zhou, S. T. Zhang, J. M. Zhao, Z. J. Wang, X. M. Ding and X. Y. Hou, *Appl. Phys. Lett.*, 2005, **87**, 044104;

45 a) S. L. Lin, L. H. Chan, R. H. Lee, M. Y. Yen, W. J. Kuo, C. T. Chen and R. J. Jeng , *Adv. Mater.*, 2008, **20**, 3947; b) W. J. Li, D. D. Liu, F. Z. Shen, D. G. Ma, Z. M. Wang, T. Feng, Y. X. Xu, B. Yang and Y. G. Ma, *Adv. Funct. Mater.,* 2012 , **22** , 2797; c) Y. Zhang, S. L. Lai, Q. X. Tong, M. F. Lo, T. W. Ng, M. Y. Chan, Z. C. Wen, J. He, K. S. Jeff, X. L. Tang, W. M. Liu, C. C. Ko, P. F. Wang and C. S. Lee, *Chem. Mater.*, 2012, **24**, 61; d) D. H. Yu, F. C. Zhao, Z. Zhang, C. M. Han, H. Xu, J.

Li, D. G. Ma and P. F. Yan, *Chem. Commun.* 2012, **48**, 6157; e) J. Ye, Z. Chen, M.-K. Fung, C. Zheng, X. Ou, X. Zhang, Y. Yuan and C.-S. Lee, *Chem. Mater*. 2013, **25**, 2630 ; f) J.-Y. Hu, Y.-J. Pu, F. Satoh, S. Kawata, H. Katagiri, H. Sasabe and J. Kido, *Adv. Funct. Mat.,* 2014, **24**, 2064.

46 R. G. Kepler, P. M. Beeson, S. J. Jacobs, R. A. Anderson, M. B. Sinclair, V. S. Valencia and P. A. Cahill, *Appl. Phys. Lett.*, 1995, **66**, 3618.

47 R. Allmann, Z. Kristallogr, Kristallgeom, Kristallphys and Kristallchem. 1970, **132**, 139. CCDC reference code PYRENE01.

Tables and Figures

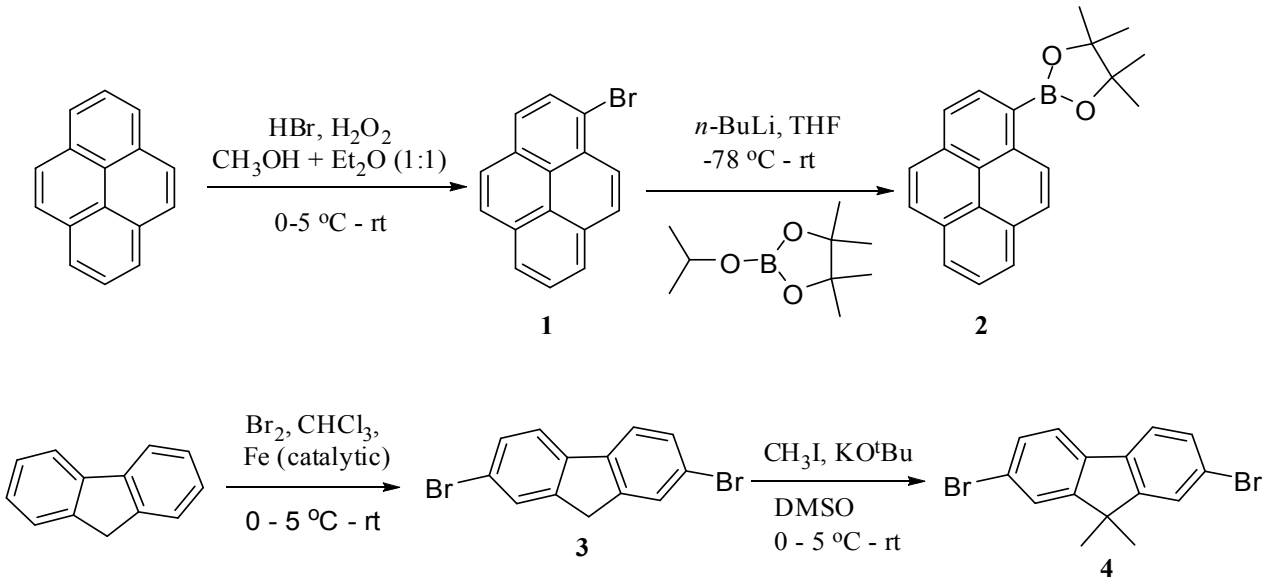

Scheme 1. Synthetic route for intermediates **2** and **4**.

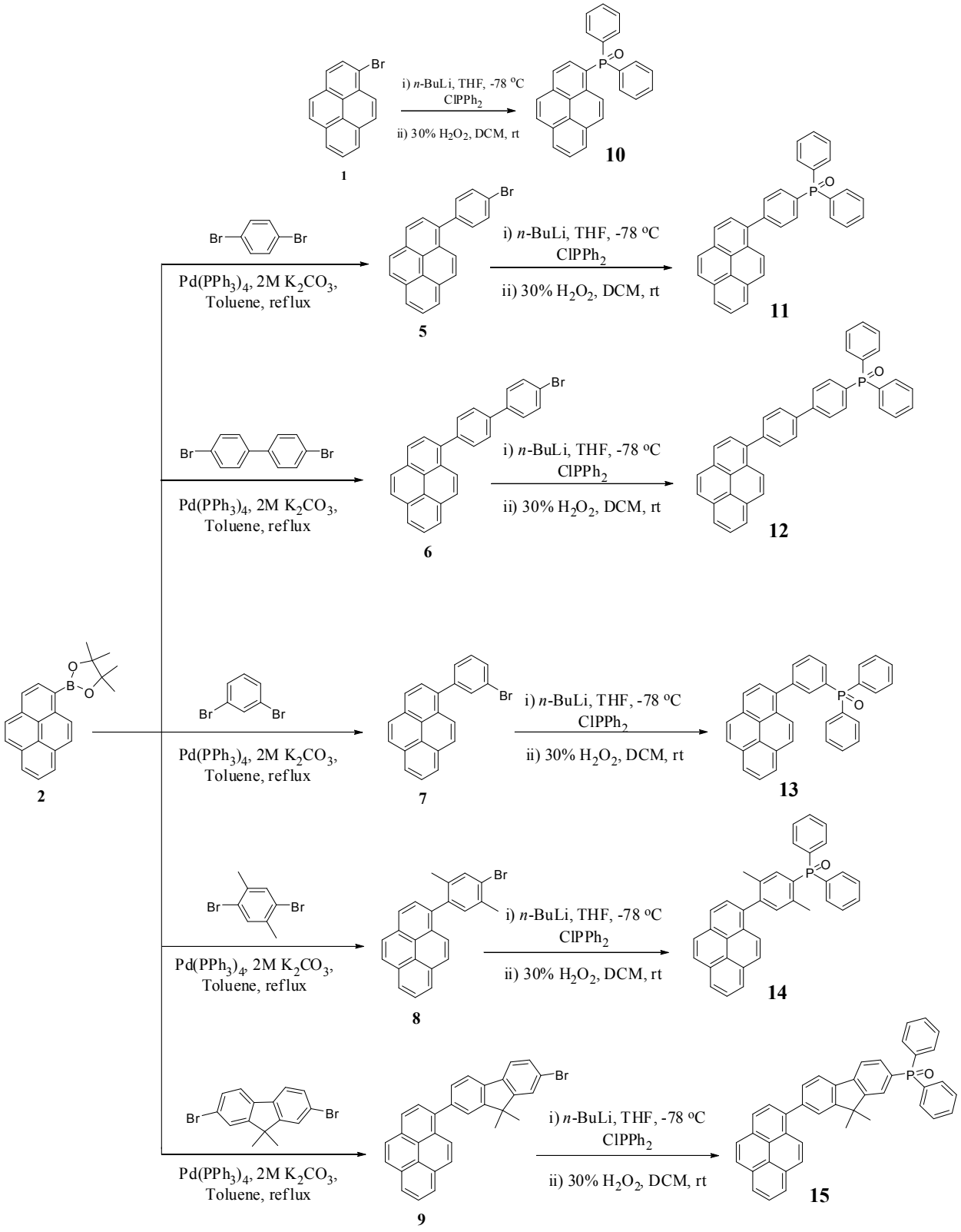

Scheme 2. Synthetic route for the six target compounds **(10-15)**.

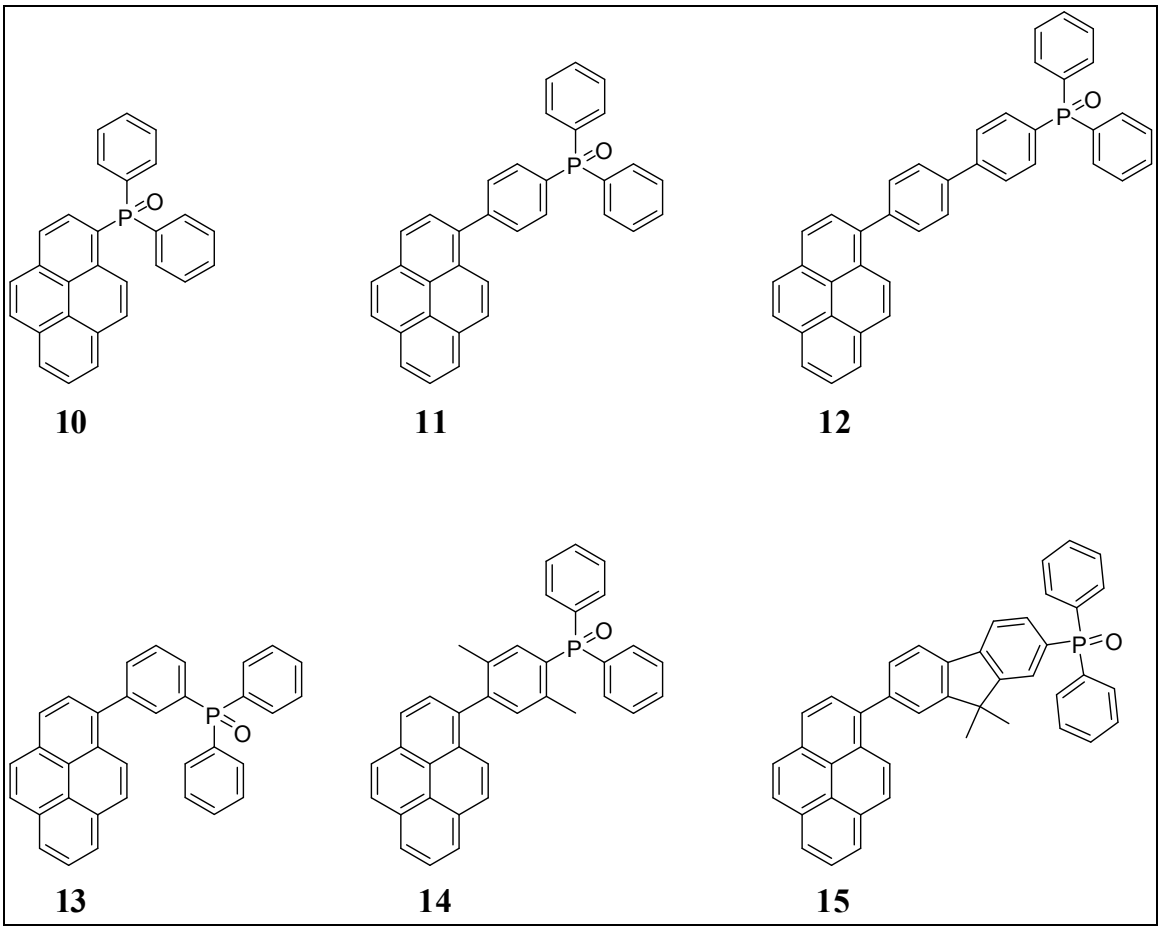

Figure 1. Molecular structures of diphenylphosphine oxide appended pyrene derivatives investigated in this work (**10-15**).

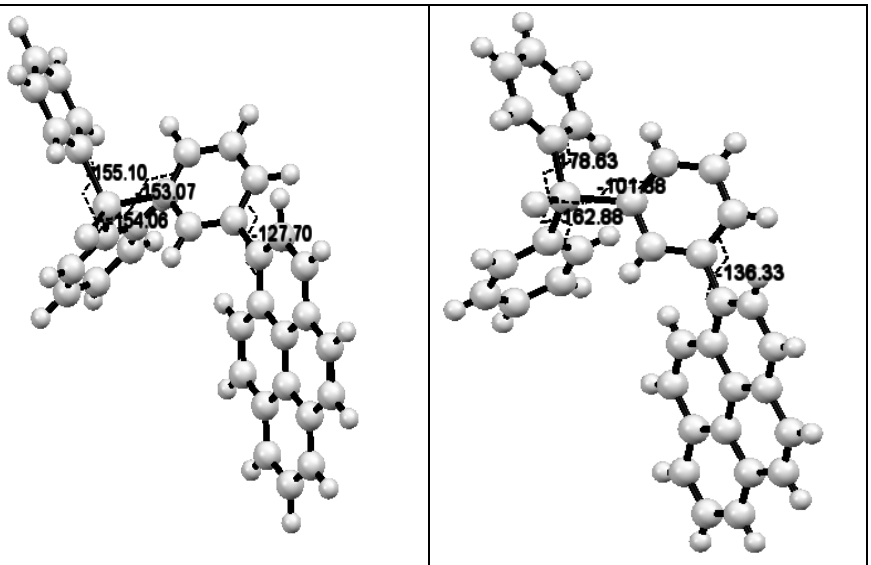

DFT optimized structure of **13**	X-ray Crystal structure of **13**

Figure 2. Molecular structure obtained using X-ray analysis and DFT-B3LYP/6-311G (d,p) optimization of compound **13**.

LUMO	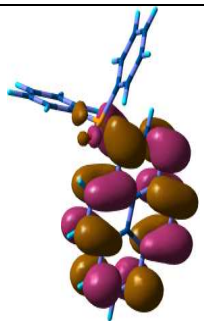	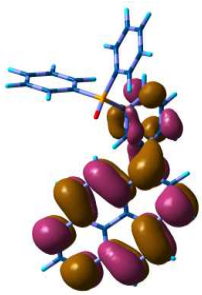	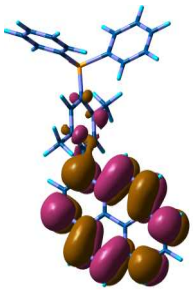	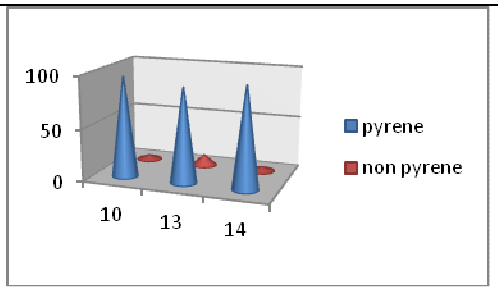
HOMO	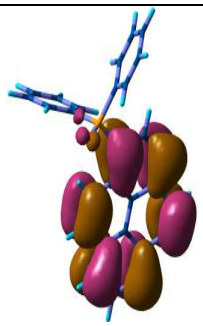	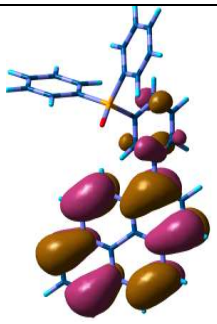	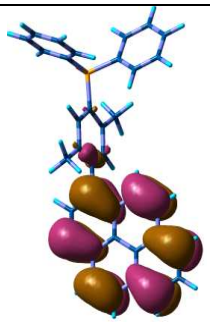	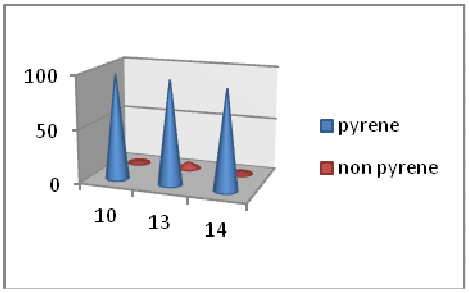
	10	**13**	**14**	Percentage contribution of functional groups to each molecular orbitals
LUMO	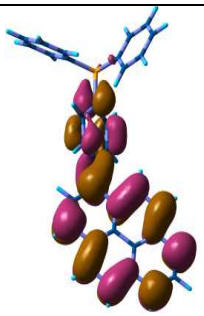	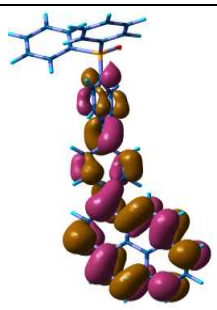	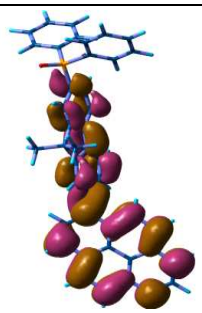	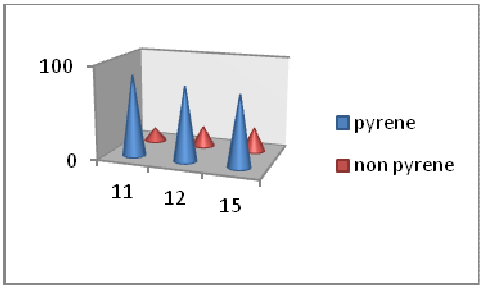
HOMO	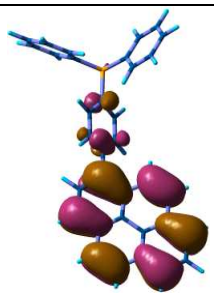	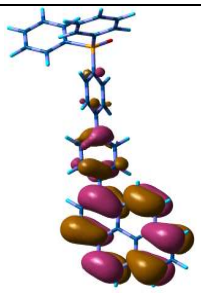	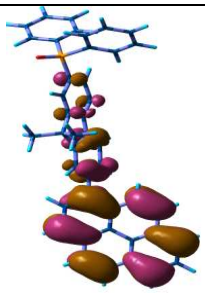	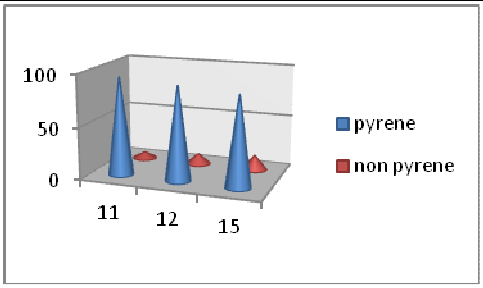
	11	**12**	**15**	Percentage contribution of functional groups to each molecular orbitals

Figure 3. Molecular orbital surfaces of the HOMO and LUMO of **10, 13, 14** (a) **11, 12, 15** (b) obtained at the B3LYP/6-311G level and graphical representation of percentage contribution of pyrene and non pyrene part to HOMO and LUMO.

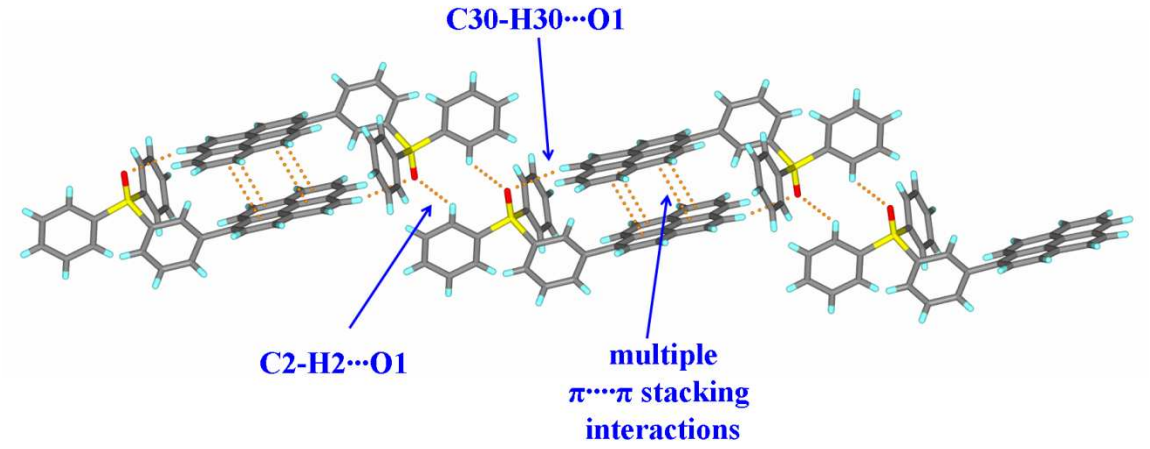

Figure 4. Crystal structure of **13** the formation of zig-zag tape via a combination of C-H···O and π···π interactions.

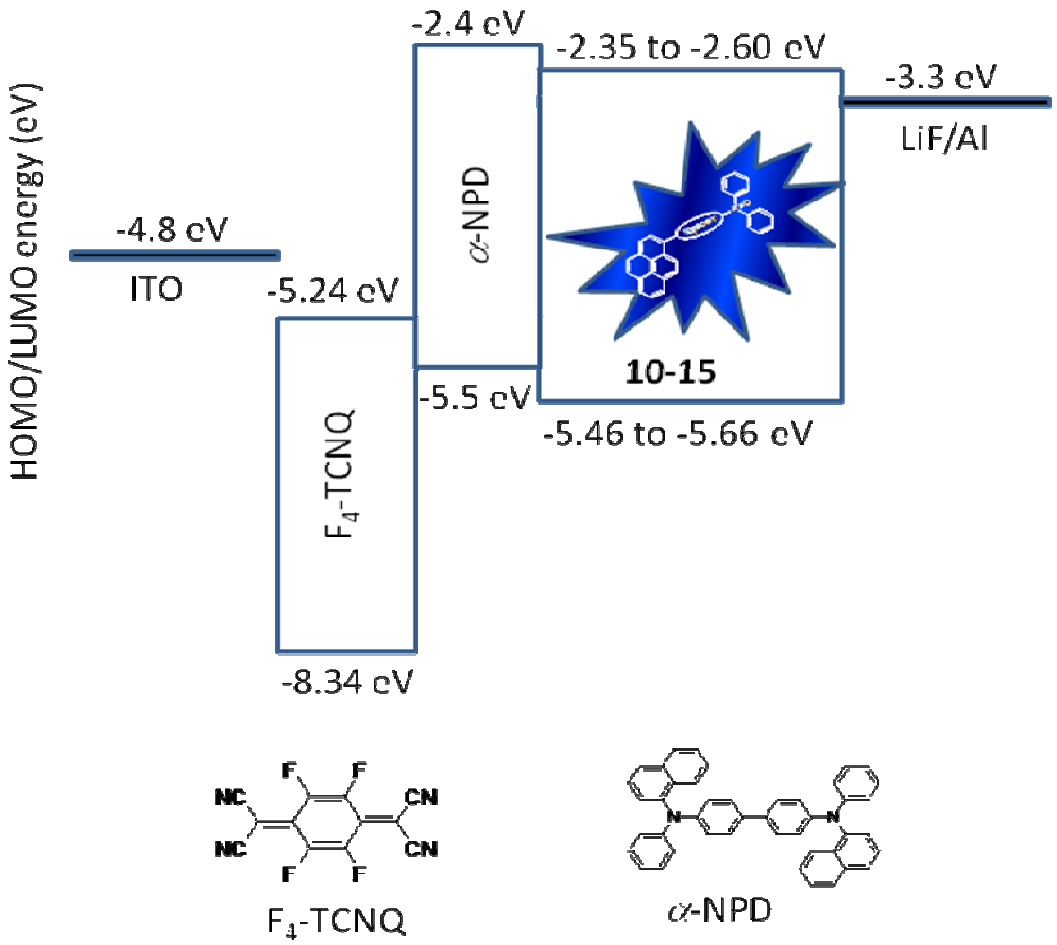

Figure 5. Typical energy level diagram for bilayer OLED with α-NPD as HTL and compounds (**10**-**15**) as n-type emitter.

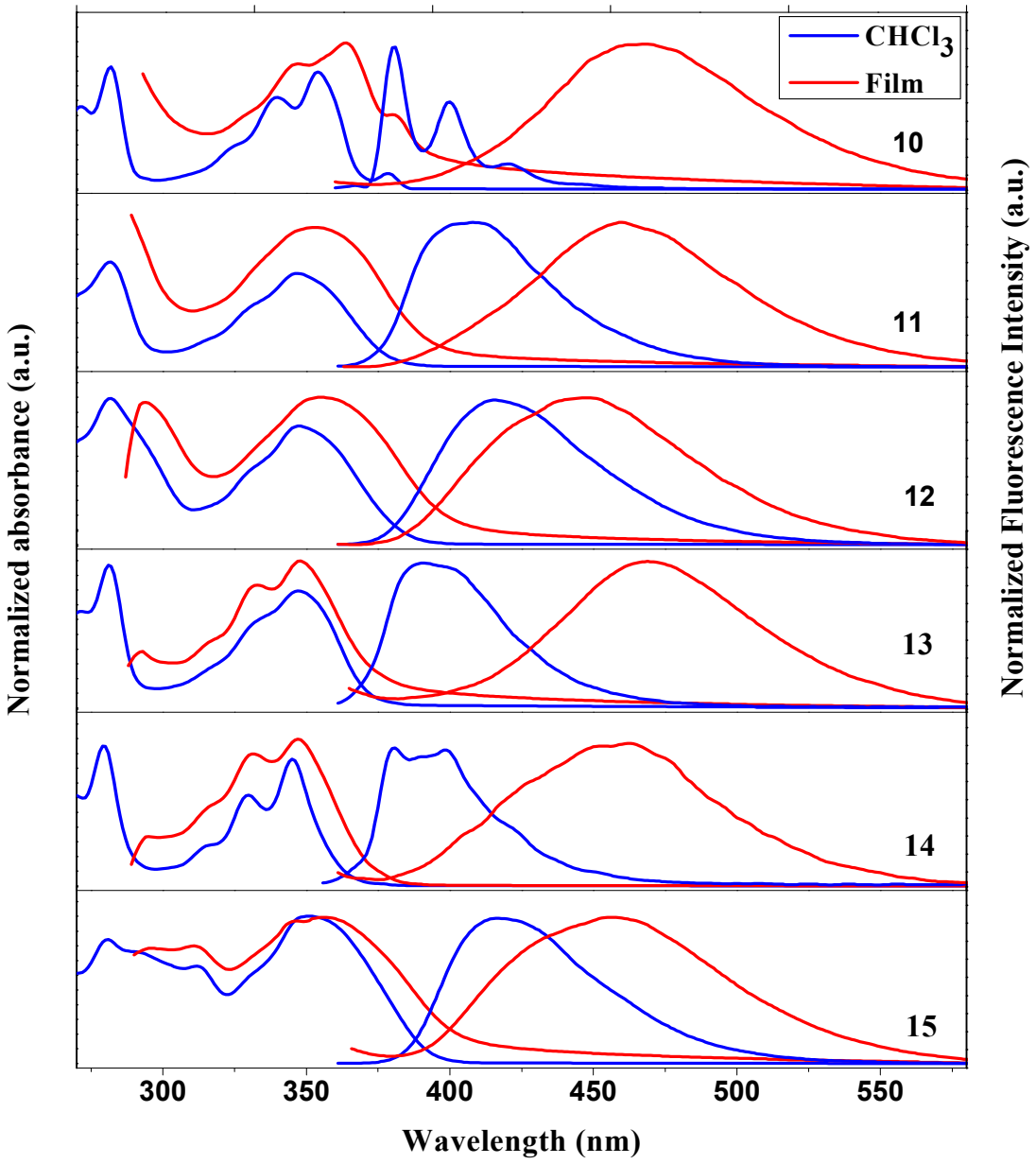

Figure 6. UV-Vis absorption and fluorescence spectra of compounds **10-15** (excited at their maximum absorption wavelength)in chloroform and thin film state.

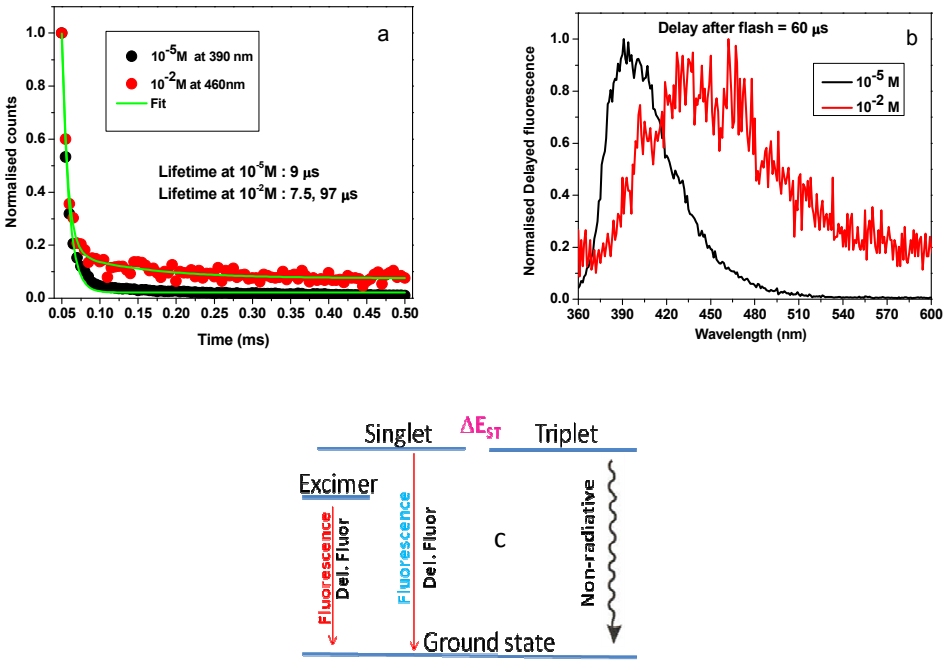

Figure 7. Fluorescence and phosphorescence spectra of **13** at RT (a) 10^{-2} M concentration; (b) 10^{-5} M concentration and (c) Energy level diagram.

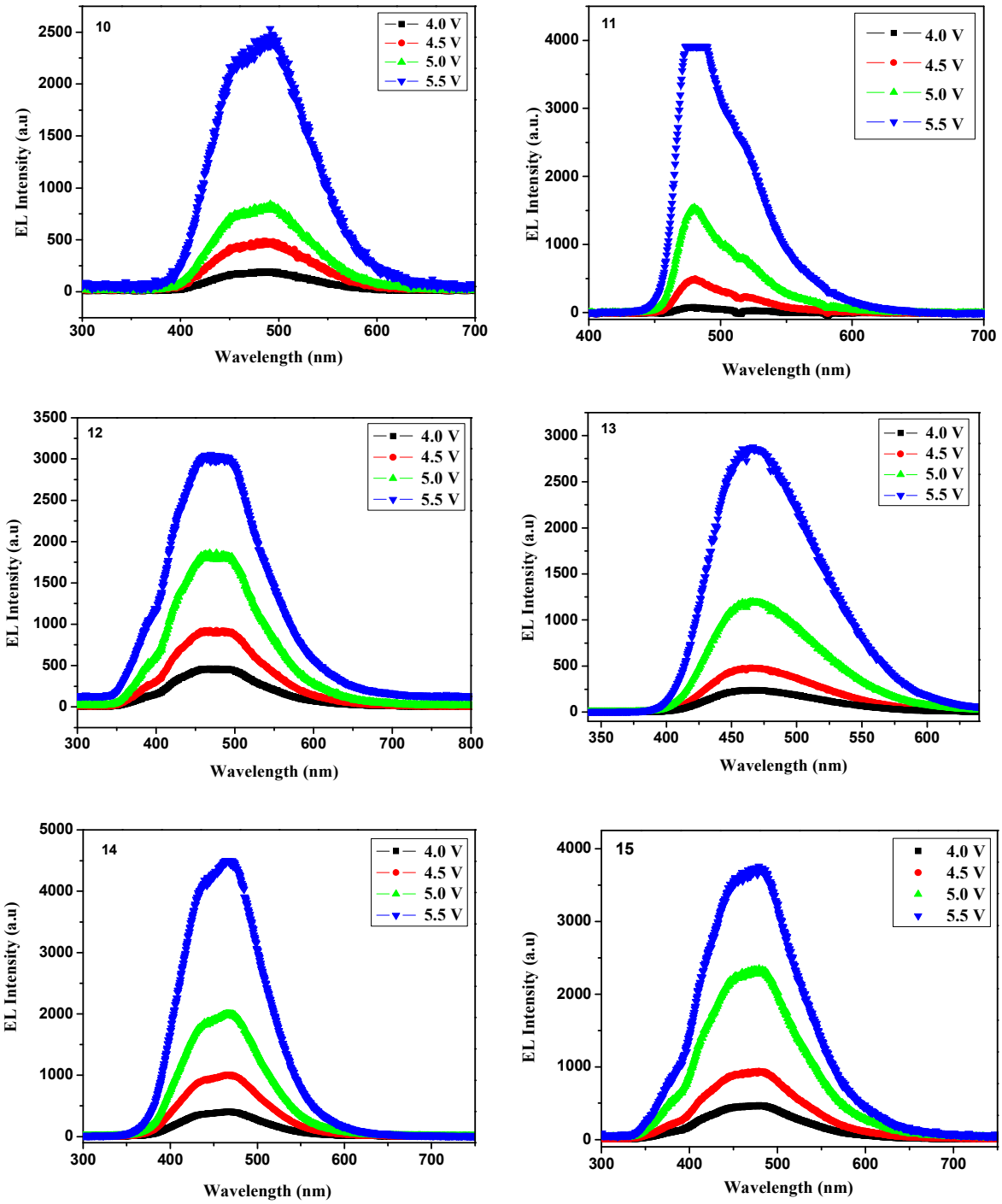

Figure 8. Electroluminescence (EL) plots of the compounds **10-15**.

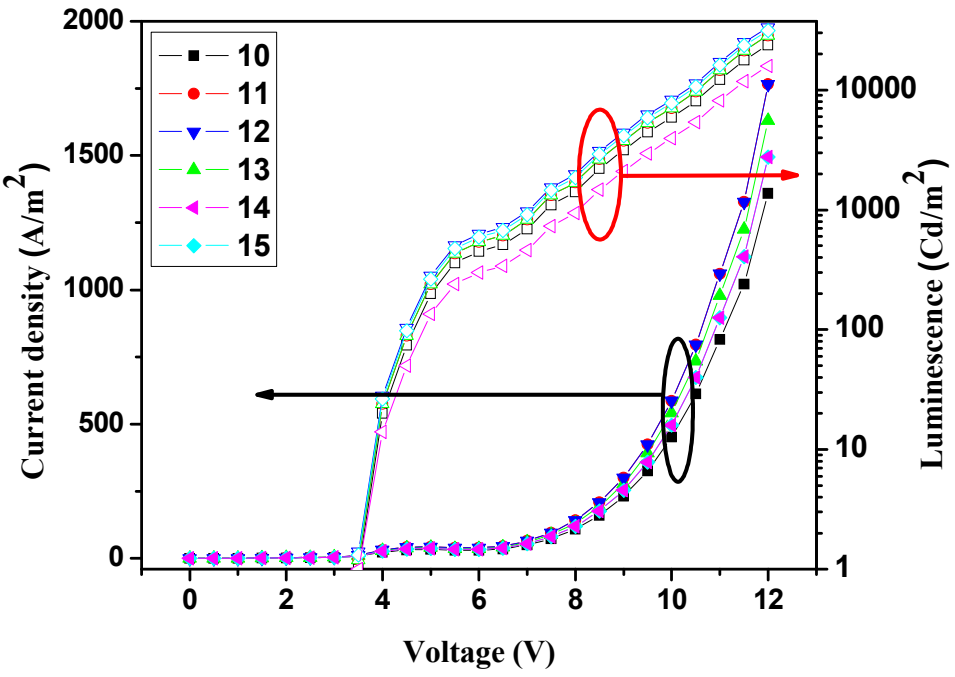

Figure 9. Current density – Voltage – Luminescence (*J-V-L*) characteristics of the compounds **10-15**.

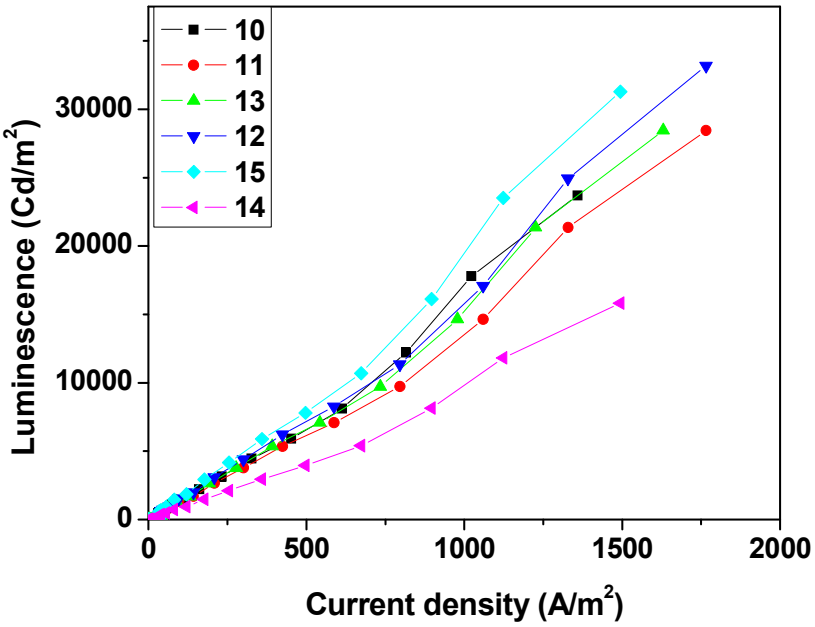

Figure 10. Current density – Luminescence (*J-L*) characteristics of the compounds **10-15**

13	Distance(A^0)	J_H	J_E	Unsubstituted Pyrene	Distance(A^0)	J_H	J_E
$t_{1,1}$	6.48	94	106	$t_{1,1}$	3.94	159	165
$t_{1,2}$	14.04	0	60	$t_{1,5}$	9.69	10	10
$t_{1,3}$	3.62	154	48	$t_{1,3}$	8.47	23	1.4

13 Unsubstituted Pyrene[28a]

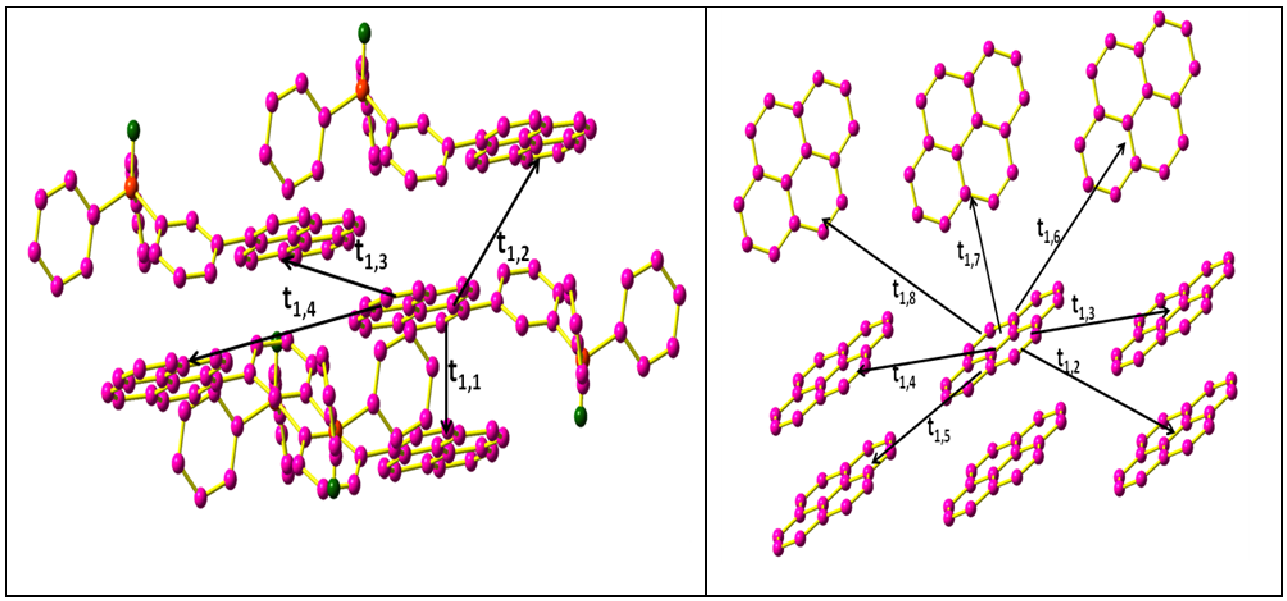

Figure 11. Estimation of Hole(J_H)and Electron transfer integrals using ADF software for **13** and unsubstituted pyrene crystal at pw91/tzp level of theory.

Table 1. Electrochemical data of the compounds **10-15**.

compound[a]	E_{ox}^{onset} (V)[b]	IP[c] (eV)	E_{red}^{onset} (V)[d]	EA[c] (eV)	HOMO[e]	LUMO[e]	μ_{ground}(D)[f]
10	1.46	5.66	-1.60	2.60	5.81	2.12	3.79
11	1.35	5.55	-1.72	2.48	5.68	2.02	3.98
12	1.34	5.54	-1.75	2.45	5.62	2.01	4.01
13	1.38	5.58	-1.80	2.40	5.58	1.93	3.77
14	1.39	5.59	-1.85	2.35	5.70	1.93	3.95
15	1.26	5.46	-1.69	2.51	5.58	2.00	3.43

[a] Cyclic voltammetry was performed to calculate IP and EA of **10-15** in THF solvent, ferrocene as internal standard electrode. [b] Onset potential of oxidation; [c] Determined from cyclic voltammetry; [d] Onset potential of reduction; [e,f] Calculated at B3LYP-6-31++G(d,p)//B3LYP-6-311G(d,p) level of theory.

Table 2. Photophysical properties of **10-15**.

Comp.	λ_{abs}[a] (nm)	Film[b] (nm)	λ_{em}[a] (nm)	Film[b] (nm)	E_g^{opt}[c] (eV)	Φ_f[d]	λ_{abs}[e] (nm)	f[f]
10	271, 282, 325, 339, 353	292, 347, 350	380, 420	482	3.28	0.91	350	0.5607
11	270, 281, 330, 346	292, 354	410	472	3.19	0.67	355	0.6870
12	269, 281, 330, 347	296, 358	422	460	3.26	0.87	362	0.9129
13	272, 281, 330, 348	291, 354	390	470	3.27	0.54	354	0.6310
14	269, 279, 315, 330, 345	334, 350	400	460	3.38	0.51	341	0.5643
15	268, 280, 312, 351	360	416	458	3.10	0.88	368	1.0492

[a] Recorded in $CHCl_3$ (1×10^{-5} M solution). [b] Recorded in thin film state. [c] Optical band gap estimated from the intersection point of the absorption-emission spectra. [d] Fluorescence quantum yield measured in chloroform using quinine sulphate (quantum yield: 0.53 (in 0.1 N H_2SO_4) as standard. [e] UV-Vis absorption spectra simulated at pbe0/6-311g(d,p) level of theory in $CHCl_3$; [f] f is oscillator strength.

Table 3. Fluorescence data of compounds **10-15** in different solvents (1 x 10^{-5} M).

Comp.	Hexane (nm)	Toluene (nm)	$CHCl_3$ (nm)	EtOAc (nm)	DMF (nm)	CH_3CN (nm)	CH_3OH (nm)
10	379, 398, 420	380, 400, 420	380, 400, 420	379, 398, 420	380, 399, 420	379, 398, 420	379, 399, 420
11	391	397	410	406	409	409	415
12	413	415	422	416	431	427	435
13	391	391	390	391	390	389	391
14	398	398	400	399	401	400	399
15	411	414	416	415	428	423	430

Table 4. Thermal data of **10-15**.

Compound	T_d (^oC)	T_m (^oC)	T_g (^oC)
10	341	243	73
11	390	208	84
12	442	244	104
13	387	196	80
14	375	188	112
15	444	273	125

T_d: Decomposition Temperature (corresponding to 5% weight loss); T_m: Melting Point; T_g: Glass Transition Temperature.

Table 5. EL performance data of the **10**-**15** as an electron transport emitter.

Device[a]	V_{on}[b] (V)	λ_{max}[c] (nm)	L_{max}[d] (cd/m^2)	η_c[e] (cd/A)	η_p[f] (lm/W)	EQE (%)[g]	μ_e[h] (cm^2/Vs)	$CIE_{(x,y)}$[i]
10	3.5	491	23700	14.6	7.65	3.3	3.2x10^{-4}	(0.18, 0.274)
11	3.5	480	28440	13.5	7.1	3.4	2.8x10^{-4}	(0.15, 0.385)
12	3.5	476	33180	15.75	8.24	3.8	4.1x10^{-4}	(0.195, 0.262)
13	3.5	467	28440	14.6	7.65	4.0	3.1x10^{-4}	(0.168, 0.227)
14	3.5	465	15800	8.86	4.64	3.0	1.2x10^{-4}	(0.156, 0.169)
15	3.5	473	31200	15.95	8.35	3.9	4.5x10^{-4}	(0.185, 0.237)

[a] Device configuration: ITO (120 nm)/F_4-TCNQ (2.5 nm)/*α*-NPD (45 nm)/Emissive layer (**10-15**) (50 nm)/LiF (1 nm)/Al (150 nm): F_4-TCNQ is an interface layer to improve the hole injection from ITO. We may consider it as an electrode with ITO; [b] Onset voltage corresponding to 1 cd/m^2; [c] Maximum wavelength; [d] Maximum brightness; [e] Maximum current efficiency at 6 V; [f] Maximum power efficiency at 6 V; [g] Maximum external quantum efficiency at 6 V; [h] Electron mobility at an electric field of 1 x 10^5 V/cm; [i] CIE coordinates.

Table 6. The EL performance data of **10**-**15** as an emitter.

Device[a]	V_{onset}[b] (V)	L_{max}[c] (cd/m^2)	η_c[d] (cd/A)	η_p[e] (lm/W)	EQE (%)[f]
10	3.5	28500	22.8	11.94	7.4
11	3.5	34300	21.1	11.0	7.2
12	3.5	42750	24.45	12.8	7.9
13	3.5	37050	24.7	12.94	8.0
14	3.5	34200	30.1	15.76	9.1
15	3.5	34400	24.9	13.0	8.1

[a] Device configuration: ITO (120 nm) / F_4-TCNQ (2.5 nm) / α-NPD (45 nm) / Emissive layer (**10-15**) (30 nm) / BCP (6 nm) / Alq_3 (30 nm) / LiF (1 nm) / Al (150 nm); [b] Onset voltage corresponding to 1 cd/m^2; [c] Maximum brightness; [d] Maximum current efficiency at 6 V; [e] Maximum power efficiency at 6 V; [f] Maximum external quantum efficiency at 6 V.

GRAPHICAL ABSTRACT

Phosphine Oxide Functionalized Pyrenes as Efficient Blue Light Emitting Multifunctional Materials for Organic Light Emitting Diodes

G. Mallesham,[1,2] Ch. Swetha,[1,2] S. Niveditha,[2] Maneesha Esther Mohanty,[1] N. Jagadeesh Babu,[3,*] Arunandan Kumar,[4,*] K. Bhanuprakash [2,5,*] and V. Jayathirtha Rao ,[1,5,*]

Electron transporting blue emitting material is obtained by end capping an electron transport enhancing group to a blue light emitting molecule. The strong interactions in the material due to the polar group and π–π stacking of the emitter lead to enhanced charge transport and efficient emission from the excimers assisted by TADF.